Front. Chem. Sci. Eng. 2025, 19(7): 63
https://doi.org/10.1007/s11705-025-2572-z

REVIEW ARTICLE

Single-atom alloys for sustainability-related electrocatalytic applications

Mingming Yin[1], Yunfei Gao[1], Chenchen Cui[1], Wei Ma[1], Li-Li Zhang (✉)[1], Zhen Zhou (✉)[1,2]

1 Interdisciplinary Research Center for Sustainable Energy Science and Engineering (IRC4SE^2), School of Chemical Engineering, Zhengzhou University, Zhengzhou 450001, China
2 National Key Laboratory of Special Rare Metal Materials, Zhengzhou University, Zhengzhou 450001, China

Abstract Single-atom alloy catalysts represent a novel and advanced category of materials in heterogeneous catalysis, attracting considerable interest in electrochemical power storage and utilization because of the distinctive structural attributes and remarkable catalytic capabilities. By establishing atomically precise arrangements of catalytic centers on metallic surfaces, single-atom alloy create highly efficient active sites with near-perfect atomic utilization. The robust electronic coupling and geometric interactions between the atomic-scale precision sites and the supporting metal matrix impart exceptional catalytic properties, such as improved kinetic performance, precise molecular recognition, and prolonged operational durability. In essence, the structural integrity of the isolated metal active sites in single-atom alloy, combined with their precisely tunable coordination environments, substantially boosts the electrochemical performance and catalytic efficiency. This review begins by introducing and discussing the fundamental concepts and inherent attributes of single-atom alloy. The methodological framework for single-atom alloy development was systematically examined, encompassing architectural design principles, fabrication methodologies, and analytical characterization techniques. Following this, the comprehensive summarization was conducted regarding the implementation of single-atom alloy catalysts in energy transformation technologies, with specific emphasis on fuel cells and environmentally electrochemical processes. Finally, forward-looking insights and perspectives are presented on the current challenges facing the development of single-atom alloy catalysts.

Keywords single-atom alloys, fuel cells, electrochemical reactions, electrocatalysts, conversion efficiency

Received March 11, 2025; accepted April 23, 2025; online June 16, 2025

E-mails: llzhang@zzu.edu.cn (Zhang L. L.),
zhenzhou@zzu.edu.cn (Zhou Z.)

1 Introduction

Energy crisis has surfaced as one of the most pivotal challenges confronting the global landscape, driven by the swift expansion of the world economy and the unrelenting increase in population [1]. Currently, over 80% of global energy demand is met by the traditional fossil fuels, primarily coal, petroleum, and natural gas [2]. The overexploitation and excessive utilization of these conventional energy sources have jointly exacerbated resource depletion and triggered significant environmental issues [3]. Consequently, the advancement and deployment of renewable energy sources have become essential to addressing the energy crisis. The adoption of sustainable energy options, including solar, wind, and hydroelectric power, can diminish dependence on non-renewable energy resources and has achieved remarkable progress over the past few decades. Nevertheless, the renewable energy presents substantial challenges to completely replacing fossil fuels in human society owing to the inherent instability, intermittency, and uneven geographical distribution [4]. Electrochemical energy conversion and storage have arisen as a profoundly promising strategy to tackle the current challenges, serving as a critical technology to facilitate the energy transition, improve the efficient utilization of clean energy, and achieve sustainable development goals. Furthermore, this approach enables the effectively regenerative electricity storage while facilitating the simultaneous conversion of waste gases, such as carbon dioxide and nitrogen oxides (NO_x), into high-economic-value chemicals and energy carriers, thereby contributing to a circular and sustainable energy economy. However, the electrochemical technologies pertinent to these conversion reactions remain in the nascent stages of development, including water splitting [5,6], fuel cells [7,8], carbon dioxide reduction reaction (CO_2RR) [9,10],

nitrogen reduction reaction (NRR) [11,12], and NO_x^- reduction to NH_3 [13,14]. The rational selection and systematic design of electrocatalysts are pivotal in facilitating these conversion reactions. Through meticulous optimization and strategic engineering of electrocatalysts, substantial enhancements in electrochemical reaction performance can be achieved, thereby offering robust support for the advancement of novel energy technologies.

The performance of electrocatalysts is comprehensively evaluated through three critical descriptors: activity, stability, and selectivity, which collectively determine the overall efficiency and operational durability of electrocatalysts in practical applications. The activity of electrocatalysts is the core index to measure the performance, with enhancement strategies primarily categorized into two distinct approaches: optimizing the natural efficiency of specific active centers and increasing the concentration of these sites [15]. The intrinsic activity of specific reaction sites is fundamentally determined by the electronic structure and coordination environment. In general, strategies such as alloying [16,17], defect engineering [18,19], and crystal phase modulation [20,21] have been extensively employed to fine-tune the electronic configuration of catalysts, thereby enhancing the intrinsic electro-activity. Additionally, precise optimization of the adsorption energy barrier also can be realized by strategically modulating the valence structure of catalysts through approaches such as heteroatom doping (e.g., nitrogen, sulfur, or phosphorus) or constructing well-defined single-atom catalytic sites, thereby enhancing the overall electrocatalytic performance [22−24]. Simultaneously, coupling strategies to increase the density of active centers represent a crucial approach for boosting the catalytic efficiency of the electrode. This can be achieved through rationally tailoring the dimensions, morphology, and architecture of nanoscale materials to obtain a high specific surface area [25,26]. Alternatively, the uniform distribution of active components across porous, high-surface-area substrates, including carbon nanotubes and graphene-based materials, has proven to be an effective strategy for increasing the number of active sites [27,28]. The stability of electrocatalysts represents a critical factor in maintaining high catalytic efficiency under practical application conditions. The improvement of stability involves the design of the composition and morphology of catalysts. Regarding compositional design, precious metal materials are widely used for their excellent chemical stability and electrical conductivity under harsh electrochemical conditions [29]. Meanwhile, carbon-based materials and cheap transition metal materials have become research hotspots due to their good stability and low cost in a mild electrolyte [30]. From a morphological perspective, multi-dimensional nanostructures, including one-dimensional nanowires, two-dimensional nanotubes, and three-dimensional integrated electrode architectures constructed from lower-dimensional building blocks, have been strategically developed. These advanced configurations not only provide enhanced mechanical robustness but also effectively mitigate the detrimental effects of Ostwald ripening in 0-dimensional nanoparticle systems [31]. In electrochemical systems involving competitive reaction pathways, such as product selectivity in CO_2RR [32], the comparison between two-electron and four-electron pathways in oxygen reduction reaction (ORR) [33], and the interfering hydrogen generation process in NRR [34], the catalytic selectivity of the electrode impacts the conversion efficiency of the desired product. Consequently, catalyst design in such reactions must prioritize selectivity, as it directly governs product yield and purity by distinguishing between competing pathways. Optimizing selectivity enhances process efficiency, minimizes by-products, and reduces separation costs and environmental impact. Thus, achieving superior selectivity requires understanding reaction mechanisms and strategically tuning the catalyst's structural and electronic properties. In general, through systematic optimization of both electronic and geometric structures, electrocatalysts can achieve enhanced activity, stability, and selectivity, thereby advancing electrochemical energy conversion technologies toward greater efficiency, cost-effectiveness, and environmental sustainability.

In recent years, a notable shift has emerged toward downsizing active metal particles from the nanometer scale to sub-nanometer dimensions and ultimately to the atomic scale, aiming to amplify atomic efficiency utilization and enhance catalytic performance. This evolutionary trajectory has culminated in the emergence of single-atom catalysts (SACs), which have revolutionized the scope of interfacial catalysis by offering unprecedented opportunities for catalyst design and fundamental research. SACs are characterized by the atomically dispersed immobilization of active metal species as isolated single atoms, achieving both maximal metal dispersion and optimal atomic utilization efficiency [35]. To date, researchers have developed diverse synthetic strategies to regulate the coordination environment of the metal active centers of SACs in different ligands, including carbon materials, oxides, metals, etc. [36,37]. Though the uniform dispersion of metal atoms ensures complete isolation, this configuration may not necessarily provide optimal adsorption characteristics and electron transfer pathways for reactant molecules. Furthermore, the inherent thermodynamic instability of isolated single atoms often leads to their migration and aggregation during both synthesis and operational catalysis processes, resulting in irreversible active sites sintering and consequent structural degradation [38]. Capitalizing on the fundamental merits of standard SACs, particularly their exceptional atomic utilization, and motivated by the synergistic effects

observed in alloy materials, researchers have recently pioneered the development of single-atom alloys (SAAs) catalysts [39]. These innovative materials have rapidly emerged as a highly promising frontier in advanced catalyst design, owing to their distinctive geometric configurations and unique electronic structures that enable exceptional catalytic performance.

SAAs represent an innovative class of catalytic materials whose unique strength lies in integrating the atomically precise active sites of SACs with the structural and electronic synergies inherent to bulk alloys, achieved through the isolated metal atoms are embedded in an inert or low-reactive metal substrate lattice [40]. SAAs not only retain the maximum atomic utilization of SACs but also strategically optimize the adsorption/desorption thermodynamics of reactant molecules through interfacial coordination environments [41]. By integrating the intrinsic catalytic activity of atomically dispersed sites with the multifunctional synergies of alloy architectures, SAAs have shown exceptional potential in driving critical energy conversion processes, particularly in frontier domains including green hydrogen production, carbon neutrality cycles, and sustainable nitrogen resource management.

2 Fundamental concepts of emerging SAAs

The construction of well-defined single atomic sites is recognized as a key strategy for optimizing catalytic performance by maximizing active site exposure and atomic utilization. Typically, SACs feature isolated metal atoms anchored on non-metallic supports [42], where strong metal-support interactions prevent atomic migration while optimizing electronic structures, thereby significantly enhancing catalytic performance (Fig. 1(a)). Unlike conventional SACs with isolated metal sites, correlated SACs with tailored metal–metal interactions show better performance advantages. For example, Jiang et al. [43] prepared Ru-based SACs with precise single-atomic interdistance by means of planar organometallic molecule design and π-π-carbon nanotube confining, which effectively promoted the hydrogen evolution reaction (HER) kinetics. In contrast, SAAs are characterized by the atomic dispersion of one active metal species onto another metallic host substrate. In this structural arrangement, the low-concentration component exists as isolated single atoms embedded within the alloy framework, establishing well-defined metal–metal bonds with the host metal through strong electronic interactions. The concept of SAAs was first proposed in 2012 by Kyriakou and colleagues [44], who pioneered the stabilization of isolated Pd atoms on Cu surfaces. This groundbreaking configuration significantly reduced the energy barriers for both hydrogen adsorption and subsequent desorption processes on the Cu substrate, marking a substantial advancement in catalytic surface engineering. Compared with conventional SACs, the single atomic sites in SAAs demonstrate enhanced structural stability due to electronic modulation from the host metal substrate, and the synergistic effect between the two metallic components creates an optimized environment for heterogeneous catalytic processes. In contrast to conventional alloy catalysts, SAAs achieve maximal atomic utilization while preserving the free-electron-like characteristics of the metallic system. Furthermore, the unique spatial separation of active sites in SAAs enables distinct metal centers to independently facilitate reactant molecule activation and intermediate adsorption, thereby surpassing the linear correlation between activation barrier and adsorption interaction. This distinctive feature ultimately leads to enhanced catalytic conversion efficiency [41]. Therefore, SAAs have been considered as a transformative platform in electrochemical interfacial catalysis, owing to their unique ability to synergistically integrate the advantageous features of both alloy catalysts and SACs.

Generally, the reactive metal species are distributed as isolated atoms over the comparatively inactive host metal substrate in SAAs. As illustrated in Fig. 1(b), the host metals typically consist of catalytically inert economical metals such as Cu, Au, and Ag, while the dopant active components are mainly composed of platinum group metals and selected transition metals [45]. This doping configuration significantly enhances the catalytic performance of the covalent metals that inherently exhibit limited reactivity but demonstrate high selectivity (e.g., Cu, Au, and Ag) [46−48]. A synergistic effect may exist between the isolated single metal atoms and the host metal sites in SAAs, which modulates the binding strength of reaction intermediates, thereby facilitating efficient catalytic processes. Furthermore, even a minimal incorporation of isolated single metal atoms can induce significant alterations in the atomic arrangement of the carrier metal surface, thereby regulating the overall catalytic performance [49]. Generally, the construction of SAAs primarily counts on the atomic dispersion of isolated metal atoms on a metallic support while simultaneously preventing both sintering and alloying processes. This process presents significant technical challenges, particularly in achieving stable anchoring of two distinct metallic species to facilitate the successful formation of SAAs. The stability of SAAs is fundamentally governed by the aggregation energy (ΔE_{agg}) of the catalytically active metal atoms on the host metal surface. Darby et al. [50] designed stable SAAs by calculating ΔE_{agg} values, which served as predictive indicators for the tendency of metal species to either disperse or aggregate on specific crystallographic planes, particularly the (111) surface. As shown in Fig. 1(c),

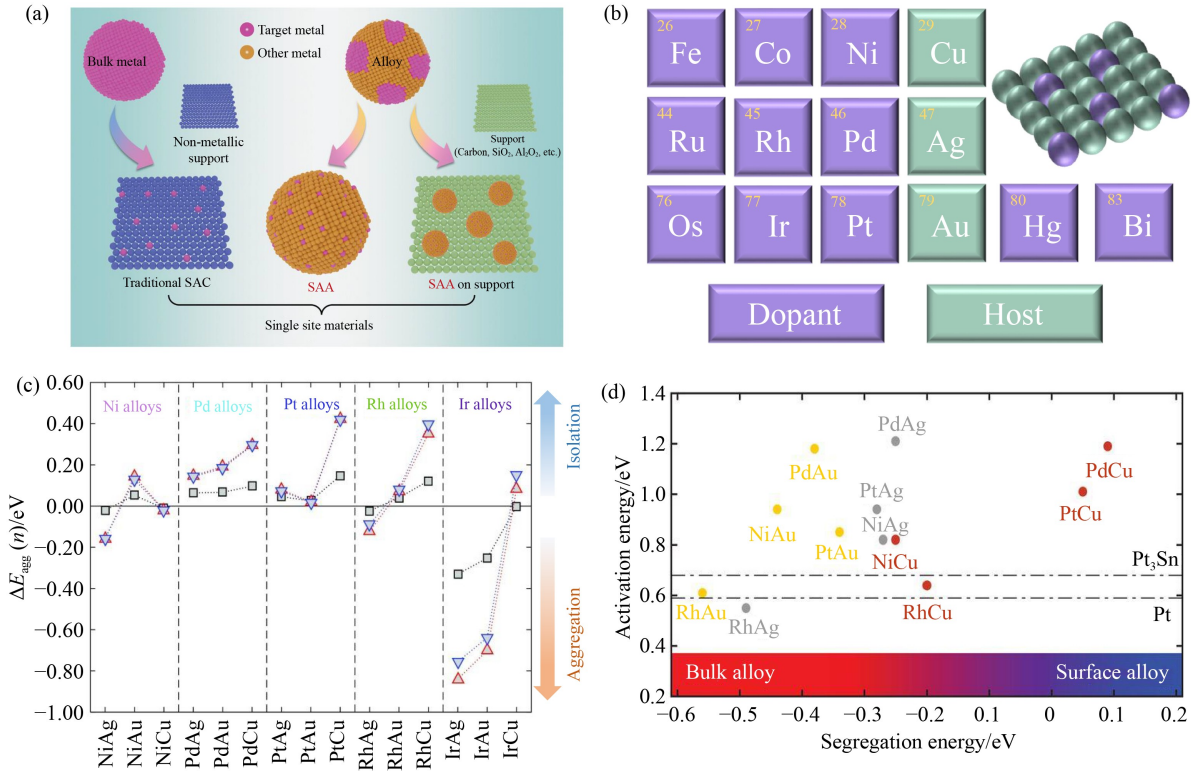

Fig. 1 (a) Diagram from conventional SAC and alloy compositions to SAA. Reprinted with permission from Ref. [42], copyright 2024, Wiley-VCH. (b) The main host and dopant elements in SAAs for electrocatalytic applications. (c) Density functional theory (DFT) predictions on which metal combinations are thermodynamically favorable for SAAs formation. The $\Delta E_{agg}(n)$ relative to the SAA phase is shown for the clustering of group 10 dopant atoms on the (111) surface of group 11 metals. Reprinted with permission from Ref. [50], copyright 2018, Springer. (d) Plot showing the activation energy for the activation and segregation energies for the initial C–H cleavage in the methane activation process of each SAA. For comparison, activation energies for Pt (111) and Pt_3Sn (111) are depicted as dash-dotted lines. Reprinted with permission from Ref. [52], copyright 2021, American Association for the Advancement of Science.

positive values indicated a thermodynamic tendency for the active metal species to disperse atomically across the host metal surface, whereas negative values suggested a likelihood of surface clustering. The computational analysis of ΔE_{agg} revealed distinct preparation feasibility, demonstrating that Pt- and Pd-based SAAs exhibit significantly higher formation probability compared to Ir-based SAAs on Au, Ag, and Cu (111) surfaces. Furthermore, the theoretical calculations of activation barrier and segregation threshold are instrumental in navigating the development of highly efficient and robust SAAs catalysts. The segregation energy is a critical parameter governing the stability of the catalyst, indicating the likelihood of dopant atoms diffusing from the surface into the interior of the host meta [51]. As illustrated in Fig. 1(d), Hannagan et al. [52] calculated the activation and segregation energies of various SAAs catalysts for the initial C–H cleavage in the methane activation process, and RhCu SAAs exhibited the most advantageous combination of enthalpy and segregation intensity among all the screened combinations. This positioned RhCu as a highly promising candidate SAAs catalyst for the alkane dehydrogenation reaction. In summary, SAAs catalysts can be systematically screened and optimized by integrating theoretical calculations with experimental validation to achieve their wide application in the field of electrochemical energy storage.

3 The structural construction of SAAs

3.1 Synthetic strategies

Developing facile and efficient synthesis methods of SAAs represents a critical step toward their practical development in large-scale applications. Based on the similarity between SAAs and traditional metal nanoalloys, SAAs can be prepared by a series of improved methods, such as reducing the load or concentration of single atomic components on the basis of commonly used alloy preparation strategies [53]. Two fundamental principles govern the rational design of SAAs: (1) strategic dilution of dopant metals to prevent cluster formation, and (2) designing the coordination environment to thermodynamically disfavor the nucleation of dopant metal ensembles [54]. In this section, we systematically categorize and analyze

prominent SAAs synthesis strategies, including reduction, atomic layer deposition (ALD), impregnation, and galvanic replacement.

3.1.1 Reduction preparation method

Currently, reduction-based approaches have gained widespread adoption in the preparation of SAAs, with co-reduction and sequential reduction methods being the most extensively employed methodologies. The co-reduction method features the parallel dissolution of multiple metal precursors in a homogeneous solution, followed by the concurrent reduction of the metallic dopant and host matrix under appropriate conditions [55]. A representative example is demonstrated by Li et al. [56], who successfully synthesized the Sb_1Cu SAA catalyst through a co-reduction strategy, where Cu^{2+} and Sb^{3+} precursors were simultaneously reduced using $NaBH_4$ in an ice-bath environment. Through a series of characterization methods, unequivocally confirmed the atomic dispersion of Sb species within the Cu base, with no detectable Sb aggregation or cluster formation.

The sequential reduction method capitalizes on the distinct reduction potentials of different metal species or employs staggered addition of metal precursors to achieve controlled stepwise reduction (Fig. 2(a)). This method is usually combined with the non-metallic supports after the preparation of SAAs. Such a strategy effectively minimizes undesirable interfacial coordination between the isolated atomic sites and the non-metallic substrate during the synthesis process, thereby ensuring the precise construction and structural integrity of the SAA

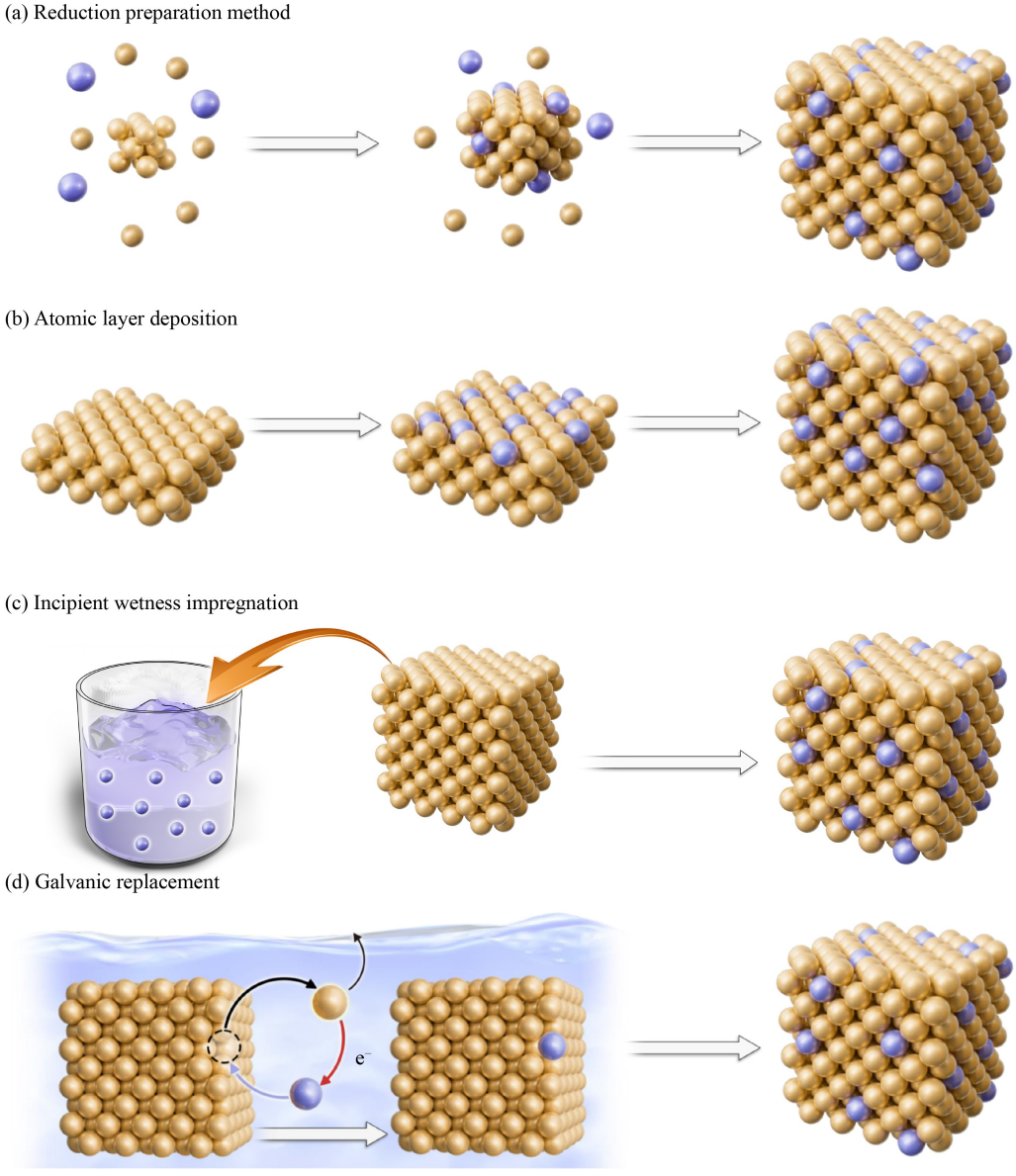

Fig. 2 Schematic illustration of four representative synthesis strategies for SAAs: (a) reduction preparation method, (b) ALD, (c) incipient wetness impregnation, and (d) galvanic replacement.

architecture. As an illustration, Ren et al. [57] successfully synthesized CuSn SAA catalyst through the reduction of an aqueous precursor mixture containing $CuCl_2$ and $SnCl_2$ using $NaBH_4$ solution. Given the more negative standard electrode potential of Sn^{2+} compared to Cu^{2+}, the reduction process proceeded sequentially: Cu^{2+} ions were preferentially reduced and followed by deposition of isolated Sn atoms on the surface or in the adjacent of Cu atoms. This work employed the simultaneous introduction of dual metal precursors while exploiting their intrinsic electrochemical potential differences to facilitate controlled sequential reduction. Utilizing precious metals (e.g., Au) as substrates, the sequential reduction approach demonstrated exceptional efficacy in precisely depositing trace amounts of dopant metals onto pre-fabricated host metal nanoparticles [58,59]. The synthesis protocol typically involved the initial formation of Au nanoparticles through thermal reduction of $HAuCl_4$ precursor at 90 °C within a sodium bicarbonate containing ethylene glycol medium. Subsequently, controlled amounts of dopant metal precursors, along with their corresponding reducing agents, were introduced through a sequential reduction process. This methodology yields unsupported bimetallic nanoparticles dispersed in the ethylene glycol medium, which can subsequently be immobilized onto various support materials as required [45,60].

3.1.2 ALD

ALD represents a sophisticated chemical vapor phase deposition technology characterized by its self-limiting surface reactions [61]. As illustrated in Fig. 2(b), in a standard ALD cycle, gaseous precursors are sequentially introduced into the deposition chamber, where they undergo surface-mediated chemical reactions with the substrate to form a monolayer. Following each precursor exposure, the system undergoes an inert gas purge to remove unreacted precursor molecules and reaction byproducts, thereby ensuring surface cleanliness for subsequent cycles. This unique growth mechanism, achieved through alternating precursor pulses separated by inert gas purging, enables the precise deposition of individual atomic layers with sub-nanometer accuracy. Through systematic repetition of these cycles, thin films with controlled thickness and composition can be fabricated on the substrate surface, where the final film thickness is accurately determined according to the number of deposition cycles performed [62]. Recently, ALD has demonstrated considerable advantages in the synthesis of SAAs, particularly in three key aspects. Firstly, ALD enables atomic-level precision control, ensuring uniform dispersion of isolated metal atoms within the SAAs matrix. Secondly, this technique offers exceptional controllability, allowing for precise regulation of SAAs structure and composition through meticulous adjustment of deposition cycles and reaction parameters, thereby facilitating controlled deposition of isolated metal atoms dispersed on the substrate. Thirdly, ALD exhibits remarkable deposition uniformity, making it particularly suitable for coating catalyst supports with complex geometries and high surface area structures [63,64]. Wang et al. [65] prepared the Pd_1Ni SAAs catalyst via the ALD method. Initially, Ni/SiO_2 catalyst with an average particle size of 3.5 nm was synthesized. Subsequently, Pd atoms were selectively deposited onto Ni nanoparticle surfaces using a low-temperature region-selective deposition strategy, ensuring no nucleation occurred on the SiO_2 support. The surface distribution of Pd atoms on the Ni nanoparticles was precisely regulated through adjustment of ALD cycle repetitions. The low-temperature deposition feature of ALD effectively inhibited metal atom migration and agglomeration, thereby maintaining the monoatomic dispersion state. In another example, Zhang et al. [66] prepared a Pt/Pd SAAs catalyst using the ALD method. Initially, Pd nanoparticles were dispersed on a silicon wafer substrate, followed by the traditional Pt ALD process, which alternated between the $MeCpPtMe_3$ precursor and O_2. After several Pt ALD cycles, Pt atoms were effectively deposited on the crystalline facets of the Pd nanoparticles. In conclusion, ALD provides exceptional control over atomic-level dispersion, structural uniformity, and compositional precision, thereby establishing itself as a highly promising strategy for customizing and preparing SAAs.

3.1.3 Incipient wetness impregnation

The incipient wetness impregnation method has attracted considerable interest owing to its straightforward methodology and remarkable efficiency. In recent years, this strategy has been effectively adapted for SAAs preparation [67]. As shown in Fig. 2(c), impregnation method refers to mixing the metal precursor with the carrier, adsorbing the metallic dopant precursor solution on the main metal or oxide substrate, followed by material drying and following treatment, including pyrolysis and reduction to remove the residual solvent to obtain the catalyst [68]. However, a critical challenge in SAAs synthesis lies in the inherent tendency of isolated metal atoms to assemble into clusters or nanoparticles at elevated temperatures. Consequently, the primary focus in SAAs fabrication via impregnation centers on developing strategies to inhibit the aggregation of isolated metal atoms during high-temperature processing. The successful implementation of the impregnation method for SAAs synthesis is determined by the exact quantity of metal-based precursor and the optimal reaction temperature profile [69]. Wang et al. [70] constructed a noble metal/Cu SAAs through an incipient wetness impregnation. The precious metal nanoparticles (Pd, Au, Ru, Rh, Ag, Ir)/CuO complexes were prepared by

physical mixing of CuO nanosheets with prefabricated colloidal dispersions of precious metal ions, and then heat treatment with H_2/Ar at 200 °C. During this process, the reduction of CuO created a metallic environment that effectively trapped migrating noble metal atoms, thereby facilitating the transformation of NM/CuO composites into well-defined NM/Cu SAAs. Furthermore, Sheng et al. [71] successfully synthesized the Pt-Rh SAA supported on activated carbon (Pt-Rh/AC SAAs) by an incipient wetness impregnation. First, activated carbon was dispersed in deionized water to form a suspension, and Pt and Rh precursors were added to the suspension under a H_2 reduction atmosphere and high temperature of 80 °C. Subsequently, simultaneous reduction of Pt^{4+} and Rh^{4+} species by H_2 led to the formation of well-dispersed Pt-Rh SAA nanoparticles anchored on the activated carbon support. In summary, the incipient wetness impregnation method serves as a versatile and efficient strategy for the synthesis of SAAs, with its effectiveness critically dependent on the precise regulation of metal precursor quantities, reaction temperatures, and reduction conditions.

3.1.4 Galvanic replacement

The galvanic replacement method exploits the inherent differences in reduction potentials between distinct metallic species to facilitate the substitution of dopant metal atoms at specific sites within the host metals (Fig. 2(d)). This approach is widely regarded as one of the foremost efficient strategies for synthesizing SAAs, which is enabled by the spontaneous reactivity under benign conditions and significant capability in the preparation of stable isolated metal atoms [72]. Numerous critical synthetic factors significantly influence the deposition of isolated metal atoms, encompassing metal precursor concentration [73], electrochemical reduction potential values [74], and structural characteristics of the metal substrate [75]. This precise preparation approach effectively addresses the structural complexity arising from the interplay between non-metallic supports, alloys, and single-atom sites. However, the method imposes stringent requirements on the reduction potential difference between the two metals, rendering it less suitable for metal pairs with small potential disparities, thereby restricting the diversity of attainable metal combinations in SAAs. From a theoretical perspective, the chemical transformation of the precursor can proceed spontaneously at room temperature with thermodynamic favorability, provided that its standard electrochemical potential marginally exceeds that of the template metal. Furthermore, the reaction kinetics demonstrate a direct correlation with the magnitude of the potential difference, where greater disparities result in accelerated reaction rates. Specifically, Luo et al. [76] obtained single-atom Rh anchored PdBi nanoplates (denoted as PtBi@Rh_1) through a galvanic replacement reaction between Bi and $RhCl_3 \cdot 3H_2O$ precursors. Subsequent electrochemical dealloying in $HClO_4$ solution effectively removed the Bi atoms, ultimately yielding the tensile-strained PtBi@$PtRh_1$ nanostructure. In addition, Zhang et al. [77] developed a multi-step synthesis protocol involving the initial preparation of CuMgAl-layered double hydroxide, followed by thermal calcination in air to obtain CuMgAl mixed metal oxide (MMO). Subsequent reduction of Cu/MMO in a H_2/Ar atmosphere yielded Cu nanocluster-supported MMO. The final PtCu SAA was achieved through galvanic replacement deposition of isolated Pt atoms the surface of Cu nanoparticles. The research group also demonstrated the synthesis of a RuNi SAA catalyst supported on an alumina substrate [78]. A series of RuNi/Al_2O_3 bimetallic catalysts was obtained by reasonably controlling $RuCl_3$ concentration and accurately controlling Ru load (0.1–2 wt %). Notably, the successful formation of RuNi SAA catalyst was achieved when the Ru loading was maintained below 0.4 wt %. These examples highlight the exceptional versatility and precision of the galvanic replacement approach in synthesizing SAAs, demonstrating its efficacy as a robust technique for the fabrication of SAAs.

The strategies discussed for SAAs synthesis possess distinct features, with their practicality and application potential hinging on factors such as efficiency, cost, and versatility. The co-reduction method is well-suited for bulk production due to its simplicity and rapid synthesis rate. However, significant differences in reduction potentials among metal precursors can result in uneven reduction, potentially forming clusters rather than single atoms. The sequential reduction method offers precise control over the metal deposition sequence, preventing competitive reduction between metals, but it requires exacting control over reaction conditions to avoid incomplete reduction or the formation of mixed phases. ALD stands out for its uniformity through precise atomic-level control, but the high cost of equipment and slow deposition rate may preclude its use for large-scale production. The incipient wetness impregnation method is conducive to industrial-scale production. Yet, it is prone to metal atom agglomeration at high temperatures, necessitating stringent control of reduction conditions. The galvanic replacement method operates under mild conditions, making it ideal for SAAs structures. However, the strict requirements for potential differences between metal pairs limit the range of feasible combinations. In summary, the co-reduction and incipient wetness impregnation methods are suited for swift industrial-scale production, but challenges related to agglomeration need to be overcome. Sequential reduction and galvanic replacement methods shine in noble metal systems, yet their applicability is relatively constrained. ALD offers the highest precision, but its cost limits widespread use. For the future, choosing the optimal synthesis method for

particular applications is critical, and surmounting current technological hurdles will be essential for the transition of SAAs from the laboratory to industrial settings.

3.2 Characterization methods

Following catalyst synthesis, a crucial analytical phase entails the comprehensive characterization of metal single atoms, including their precise identification, spatial distribution patterns, and local coordination environments within the host metal matrix. The primary methods for characterizing single atoms include direct imaging and advanced spectral analysis of local structures. Notably, spherical aberration-corrected high-angle annular dark field scanning transmission electron microscopy (HAADF-STEM) enables the direct visualization of atomic dispersion. Additionally, extended X-ray absorption fine structure (EXAFS) spectroscopy reveals a profound understanding of coordination environments, bond distances, and electronic configurations, offering a comprehensive understanding of the atomic-scale environment. These techniques collectively form the cornerstone for elucidating the structural and functional properties of SAAs.

The microscope is considered the premier tool for describing SAAs, providing distinct confirmation of the single atoms on the carrier [79]. HAADF-STEM serves as the primary method for characterizing the structure and morphology of atomically dispersed supported catalysts. STEM employs a focused electron beam and detects high-angle scattered electrons through an annular dark-field detector, enabling atomic-scale resolution imaging through spherical aberration correction. The identification of isolated atomic sites in STEM relies predominantly on atomic number contrast, with signal intensity exhibiting a power-law dependence on atomic number [80]. HAADF-STEM enables direct visualization of the location and distribution of atomically dispersed sites in SAAs, particularly when the single atoms exhibit significantly higher atomic numbers compared to the substrate material [81]. Specifically, the HAADF-STEM image in Fig. 3(a) revealed an interplanar distance of 0.208 nm, consistent with the Cu (111) plane. Furthermore, bright monoatomic columns were observed interspersed within the Cu array highlighted by red circles in Fig. 3(b), indicating the successful doping of heavier atomic-level metals into the Cu matrix [82].

However, STEM is limited to providing morphological and dispersion information about the metal sites and cannot directly determine their chemical composition. Consequently, confirming the presence of single atoms solely through STEM is challenging. To address this limitation, STEM is often combined with energy dispersive X-ray spectroscopy (EDS) [83]. EDS operates by bombarding the sample with an electron beam, inducing the emission of characteristic X-rays, which enables qualitative compositional analysis. Atomic-resolution EDS identified the bright spots as Mo atoms, confirming their uniform dispersion within the Cu array and the successful synthesis of the Mo_1Cu SAAs catalyst in Fig. 3(c). Despite its advantages, HAADF-STEM has inherent technical limitations. For example, the interaction of high-energy electron beams with the sample can lead to beam damage, including atomic migration and bond cleavage [84]. Moreover, its limited depth of field complicates the imaging of features at varying sample depths, and it struggles to differentiate elements with close atomic numbers [85]. These limitations highlight the need for complementary techniques to fully characterize SAAs.

Although advanced STEM imaging techniques enable the direct visualization of individual atoms, they are limited to providing localized information within a specifically selected region and are insufficient for elucidating the detailed chemical environment of SAAs. In modern experimental studies, synchrotron radiation X-ray absorption spectroscopy (XAS) has evolved into a pivotal methodology for analyzing the electronic configurations and atomic-scale coordination environment of metallic centers in SAAs. XAS provides averaged information regarding the atomic coordination environment throughout the bulk sample, complementing the localized insights provided by STEM [86]. XAS is broadly categorized into EXAFS and X-ray absorption near edge structure (XANES). Techniques such as the Fourier transform (FT) and wavelet transform (WT) techniques were employed for EXAFS data analysis to serve as a qualitative implement for evaluating the coordination environment of specific atoms. These methods enable the prediction of bond distances and coordination numbers [87,88]. For instance, Fig. 3(d) shows the Ni *K*-edge spectra of $NiPt_{SA}$@NC (N-doped carbon) compared with those of NiO and Ni foils, where the binding energy of $NiPt_{SA}$@NC lies between that of NiO and Ni foil, suggesting that the Ni atoms were in a partially positively charged state. Additionally, the Pt L_3-edge XANES spectrum of $NiPt_{SA}$@NC (Fig. 3(e)) exhibited a slight reduction in white line intensity compared to Pt foil, indicating electron transfer from Ni to Pt. The FT of the Ni *K*-edge EXAFS oscillations (Fig. 3(f)) revealed a peak similar to that of the Ni foil, consistent with a Ni-Ni (or Ni-Pt) coordination environment. Furthermore, EXAFS analysis at the Pt L_3-edge (Fig. 3(g)) showed a prominent peak at around 2.2 Å, attributed to Pt-Ni coordination bond. The absence of a Pt-Pt coordination peak unequivocally confirmed the atomic dispersion of Pt within $NiPt_{SA}$@NC. WT analysis further elucidated the coordination environment of Pt in both k-space and R-space. The isocontour maps (Fig. 3(h)) demonstrated that, unlike the spectra of Ni foil, Pt foil, and PtO_2, the coordination signals for Ni-Ni (≈ 8.0 Å), Pt-Pt (≈ 12.5 Å), and Pt-O (≈ 6.8 Å) were absent in

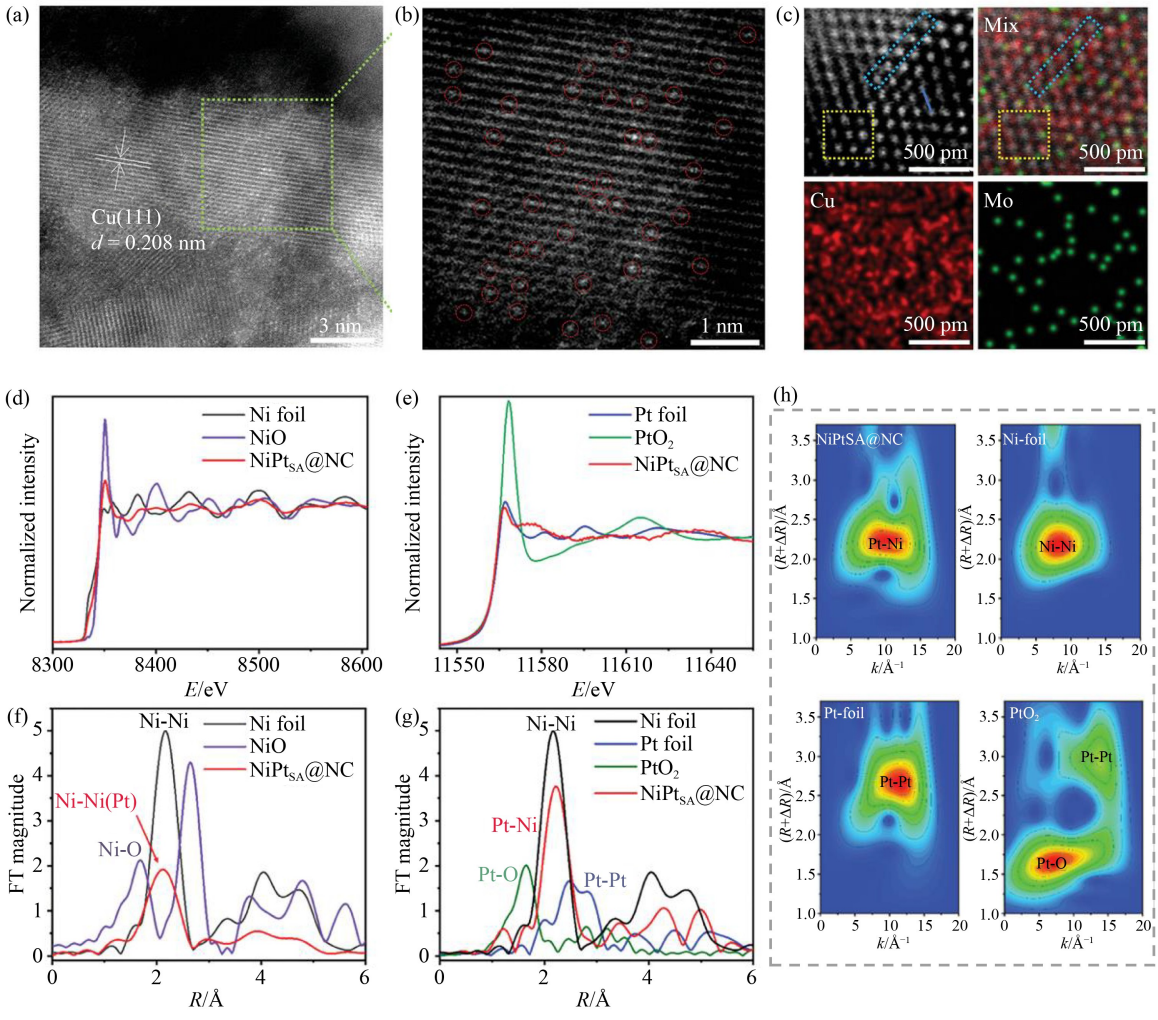

Fig. 3 (a) HAADF-STEM image of the 0.7% Mo_1Cu. (b) Zoomed-in view of the image in the panel. (c) Atomically resolved elemental mapping of the 0.7% Mo_1Cu. Reprinted with permission from Ref. [82], copyright 2025, Wiley-VCH. (d) Normalized Ni *K*-edge XANES spectra. (e) Normalized Pt L_3-edge XANES spectra. (f) FT-EXAFS curves at the Ni *K*-edge. (g) FT-EXAFS curves at the Pt L_3-edge. (h) WT of Pt *L*-edge EXAFS spectra for $NiPt_{SA}$@NC, with Ni foil, Pt foil, and PtO_2 as references. Reprinted with permission from Ref. [89], copyright 2024, Wiley-VCH.

$NiPt_{SA}$@NC [89]. This observation further corroborates that Pt atoms in $NiPt_{SA}$@NC are atomically dispersed with a predominant coordination to Ni atoms. These findings highlight the XAS spectroscopy in providing a comprehensive understanding of the coordination environment at the atomic level of SAAs.

In addition to STEM and XAS, diffuse reflectance infrared FT spectroscopy using CO as a probe molecule (CO-DRIFTS) serves as another effective technique for identifying doped single atoms [90]. Since the probe molecules are adsorbed at distinct positions with characteristic vibrational frequencies, which are highly sensitive to the adsorption model, the distribution of single atoms is capable of being determined by analyzing the adsorption/desorption behavior of CO. However, CO-DRIFTS may not produce reliable or interpretable data for metals that exhibit weak or unstable interactions with CO. Therefore, a comprehensive and accurate characterization of the structure and nature of SAAs can only be fulfilled through the integration and cross-validation of multiple characterization methods. Furthermore, a detailed evaluation of the atomic configuration before and after catalytic processes is essential for investigating the structural stability of SAAs materials under varying reaction conditions [91,92]. In this context, *in situ* characterization has emerged as a critical approach for elucidating the structural evolution and dynamic processes of SAAs during reactions, thereby providing deeper insights into their complex behavior and mechanisms.

4 SAAs for electrocatalysis

SAAs possess immense potential to supplant conventional catalysts due to their pronounced properties,

which are ascribed to the optimized atomic utilization and the robust electronic interactions between the isolated metal sites and the host metals, thus substantially achieving outstanding catalytic efficacy in a multitude of electrocatalytic reactions pertinent to energy conversion. In this section, we present an exhaustive analysis of the applications of SAAs in electrochemical energy conversion.

4.1 Fuel cells

4.1.1 ORR

Electrocatalytic ORR proceeds through two specific mechanistic pathways: (1) the direct four-electron pathway, leading to the complete reduction of oxygen to water, and (2) the sequential two-electron pathway, resulting in the generation of H_2O_2 as an intermediate product [93]. The ORR advances through direct four-electron transfer have been extensively utilized in energy conversion and storage mechanisms, particularly fuel cells and metal-air batteries. In contrast, the two-electron pathway enables the selective reduction of O_2 to H_2O_2 under ambient temperature and pressure conditions. This method offers high efficiency in H_2O_2 synthesis and is considered a promising alternative to the traditional anthraquinone method, which is associated with excessive energy consumption and significant environmental damage [94]. Typically, high-performance cathode catalysts are essential to facilitate the ORR through an efficient four-electron transfer pathway, thereby maximizing the energy conversion efficiency of the fuel cell device. This necessitates the development of advanced catalytic materials capable of enhancing both O_2 activation and O–O bond cleavage kinetics [95]. Pt-based catalysts have long been recognized as the most effective catalysts for ORR in proton exchange membrane fuel cells (PEMFCs). However, the elevated cost resulting from the scarceness of Pt resources has impeded their widespread commercialization. Therefore, designing catalysts that exhibit superior activity, stability, and cost-effectiveness represents a critical research focus in electrocatalytic ORR. Strategies such as reducing the size of Pt nanostructures and alloying have been employed to enhance Pt utilization and the intrinsic activity of catalysts [96,97]. Additionally, significant efforts are being directed toward discovering cost-effective and efficient non-precious metal catalysts as alternatives to expensive and scarce Pt-based catalysts.

SAAs represent an emerging class of heterogeneous catalysts characterized featuring well-defined active sites. Recently, researchers successfully diluted Pt atoms using low-cost metal atoms, achieving isolated single-atom Pt sites while precisely regulating the material's electronic structure and geometric configuration. This approach has enabled the design of SAAs catalysts exhibiting exceptional four-electron ORR activity. In particular, Cheng et al. [98] synthesized a range of Pt_1Co_n alloys embedded in nitrogen-doped graphite carbon nanotubes (N-GCNTs), denoted as Pt_1Co_n/N-GCNT, as SAAs catalysts for acidic ORR (Fig. 4(a)). HAADF-STEM images evidenced the dispersion of isolated Pt atoms on

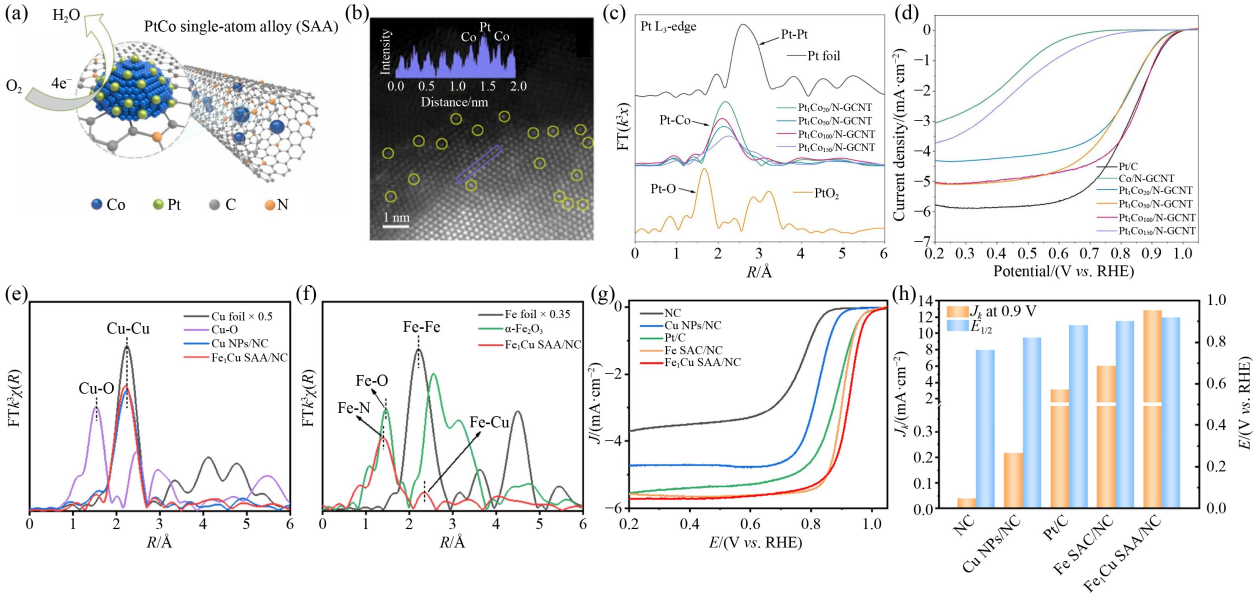

Fig. 4 (a) The schematic of Pt_1Co_n/N-GCNT encapsulated within a graphitic carbon nanotube. (b) HAADF-STEM image of Pt_1Co_{100}/N-GCNT, with the inset showing the line-scan intensity profile derived from the purple box. (c) Amplitude of the Fourier-transformed EXAFS spectra at the Pt L_3-edge. (d) Polarization curves of the ORR for various catalysts. Reprinted with permission from Ref. [98], copyright 2022, Elsevier. (e) FT k^3-weighted EXAFS spectra at the Cu K-edge. (f) FT k^3-weighted EXAFS spectra at the Fe k-edge. (g) Polarization curves measured in O_2-saturated 0.1 mol·L^{-1} KOH electrolyte. (h) Comparison of the J_k at 0.9 V and the $E_{1/2}$ for the evaluated catalysts. Reprinted with permission from Ref. [99], copyright 2024, Springer.

the surface of Co nanoparticles on the Pt_1Co_{100}/N-GCNT catalyst (Fig. 4(b)). Additionally, the Pt-Co bonding of EXAFS further indicated the effective preparation of the SAAs (Fig. 4(c)). In an acidic electrolyte, the Pt_1Co_{100}/N-GCNT SAAs catalyst exhibited outstanding ORR catalytic performance with a mass activity 5.4-fold greater than commercial Pt/C at 0.9 V *vs* reversible hydrogen electrode (RHE) in Fig. 4(d). This enhanced activity was attributed to the exceptional Pt-Co dual-site configuration in the SAAs, which induced a delocalized charge distribution. This electronic modification optimized the adsorption and regulation of O_2 dissociation energy, especially the immobilization of OOH* intermediates and the dissociation of OH* intermediates, resulting in an efficient four-electron ORR pathway. In another study, Niu et al. [99] developed a Fe-Cu dual-site SAAs catalyst supported on carbon nanosheets. As illustrated in Fig. 4(e), the slight negative shift in the Cu-Cu coordination bonds observed in Fe_1Cu SAA/NC confirmed the presence of electronic interactions between Fe and Cu atoms. These interactions were crucial for the adsorption and activation of ORR intermediates. In Fig. 4(f), the appearance of Fe-Cu coordination bonds and the absence of Fe-Fe coordination bonds further verified that Fe is located as isolated single atoms on the Cu substrate. As demonstrated in Figs. 4(g) and 4(h), the Fe_1Cu SAA/NC catalyst demonstrated outstanding ORR performance, showing only a 5 mV potential drop after 5000 cycles of durability testing. This exceptional electrochemical stability highlighted the potential of Fe_1Cu SAA/NC as an efficient and enduring ORR catalyst. The superior ORR activity of the Fe_1Cu SAA/NC originated from the Fe single atoms induced electronic redistribution at the Cu nanoparticle interface. This structural modulation synergistically optimized the binding energy of ORR intermediates while facilitating electron transfer kinetics through the reconstructed coordination environment.

SAAs demonstrate transformative potential for the ORR in fuel cells by anchoring noble metals as isolated atoms on cost-effective transition metal hosts, thereby achieving dual breakthroughs in catalytic activity and operational durability. This architecture not only dramatically reduces noble metal loading to trace levels while maintaining exceptional mass activity, but also enhances electron transfer kinetics through tailored coordination environments, as evidenced by the delocalized charge distribution at Pt-Co dual sites [98]. Despite these advances, challenges persist in scaling up synthesis protocols due to the stringent requirements for atomic-level dispersion control and risks of metal leaching under PEMFCs operating conditions. Future efforts should focus on developing universal synthesis strategies for SAAs with operando characterization techniques to elucidate dynamic interfacial processes during ORR. The unique merits of SAAs including maximum atom utilization, tunable electronic structures, and compatibility may ultimately democratize clean energy technology toward greater efficiency and accessibility.

4.1.2 Fuel oxidation reactions

For the past few years, direct liquid fuel cells (DLFCs) with small organic molecules as anodic fuels, such as methanol [100], ethanol [101], and formic acid [102], address challenges related to fuel storage and transportation. The electrochemical oxidation of these small molecules, a critical process in fuel cell technologies, predominantly depends on Pt-based catalysts. However, this dependence on precious metal catalysts increases the overall system expenses because of the inherent scarcity of Pt resources coupled with the intricate and energy-intensive fabrication processes involved in catalyst synthesis, creating significant barriers to the widespread commercialization and sustainable advancement. In addition, Pt-based catalysts are particularly susceptible to intermediate poisoning and progressive surface deactivation during extended operational periods, which substantially diminishes their cost efficiency and long-term stability in real-world applications, thereby limiting their practical utility and economic viability [103]. In recent years, SAAs catalysts have garnered widespread attention as an electrocatalyst for these carbon-containing anodizing reactions. The strategic incorporation of a secondary metal as the host matrix enables a substantial reduction in precious metal loading while regulating the adsorption affinity of the active center to CO or changing the oxidation pathway of carbon-containing reactants. Consequently, this innovative approach addresses the critical challenge of catalyst deactivation by mitigating CO poisoning effects on the catalytic interface, thereby enhancing the durability and performance of the electrocatalytic system. Theoretical calculations and experimental studies indicate that for both the methanol oxidation reaction (MOR) and ethanol oxidation reaction (EOR), a minimum of three adjacent Pt atoms are necessary to constitute an active center for the complete electrooxidation of reactants [104,105]. The EOR represents a complex 12-electron transfer mechanism that necessitates substantial energy input to facilitate C–C bond cleavage. Therefore, an ideal EOR catalyst should demonstrate dual functionality: exceptional CO poisoning resistance and the capacity to cleave C–C bonds at reduced overpotentials to promote complete ethanol oxidation [106]. In contrast, the formic acid oxidation reaction (FAOR) involves only a two-electron transfer process, resulting in significantly faster reaction kinetics compared to MOR and EOR. Typically, FAOR proceeds through two contrasting pathways, including the direct dehydrogenation pathway and the indirect dehydration pathway. The direct dehydrogenation

pathway releases H^+ without generating CO intermediates, a highly desirable characteristic that circumvents the issue of catalyst poisoning. Conversely, the indirect dehydration pathway involves the decomposition of formic acid into CO and H_2O, however, the adsorption of CO onto the catalyst results in deactivation, rendering this pathway undesirable [107].

The design of SAAs with isolated active sites is crucial to maintaining high catalytic activity and selectivity, thereby addressing the challenges associated with CO poisoning and enhancing the overall performance of DLFCs. Tilley et al. synthesized PtRu SAAs, in which isolated Pt single atoms evenly distributed across Ru nanoparticles (Fig. 5(a)) [108]. The EXAFS spectrum further confirmed the existence of Pt single atoms on the Ru nanoparticle surface (Fig. 5(b)). Electrochemical performance tests revealed that the PtRu SAAs exhibited a remarkable current density and mass activity for the MOR, as shown in Fig. 5(c). Specifically, the isolated Pt atomic structure demonstrated a strong adsorption capability for CH_3OH, which facilitated the MOR process, while simultaneously exhibiting weak binding to CO intermediates, thereby effectively mitigating CO poisoning. Wang et al. [109] prepared atomically dispersed Bi on Pd nanowires in Fig. 5(d), denoted as $IL/Pd_{50}Bi_1$ (IL: ionic liquid). Structural characterization by EXAFS spectroscopy revealed characteristic Bi-Pd and Bi-O bonds with corresponding bond lengths of 2.52 and 1.66 Å, respectively (Fig. 5(e)). The absence of Bi-Bi bonding signals at 2.9 Å in the EXAFS spectrum verified

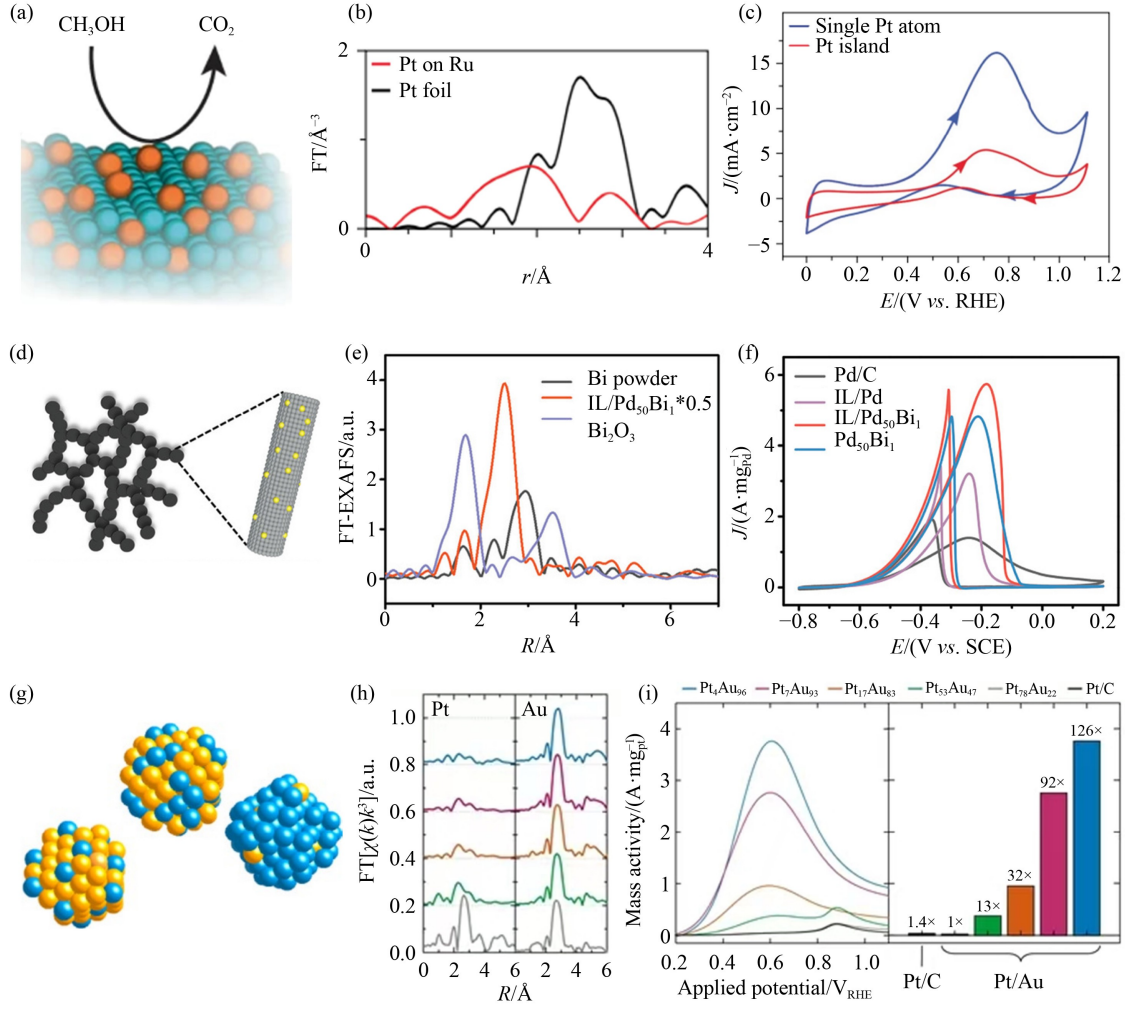

Fig. 5 (a) Schematic diagram of the single Pt atoms on Ru nanoparticles, with blue highlighting the hexagonal close packed (hcp) Ru sites and orange highlighting the face-centered cubic Pt sites. (b) FT-EXAFS spectra at the Pt L_3-edge for Pt foil and single Pt atoms on Ru nanoparticles. (c) Electrocatalytic MOR performance of single Pt atoms on Ru and Pt islands on Ru catalysts. Reprinted with permission from Ref. [108], copyright 2022, Springer Nature. (d) Schematic illustration of the $IL/Pd_{50}Bi_1$ hydrogels. (e) The k^3-weighted $\chi(k)$ function derived from the EXAFS spectra of Bi powder, Bi_2O_3, and $IL/Pd_{50}Bi_1$ aerogels. (f) CV curves of IL/Pd, $IL/Pd_{50}Bi_1$, and $Pd_{50}Bi_1$ aerogels and commercial Pd/C catalysts, measured in N_2-saturated 1.0 mol·L^{-1} KOH containing 1.0 mol·L^{-1} ethanol. Reprinted with permission from Ref. [109], copyright 2021, Wiley-VCH. (g) The schematic of PtAu SAA configuration. (h) FT-EXAFS spectra of PtAu nanoparticles at Pt and Au L_3-edges. (i) Pt mass-normalized anodic scans of PtAu nanoparticle system. Reprinted with permission from Ref. [110], copyright 2024, Springer Nature.

the atomic-level dispersion of Bi atoms within the IL/$Pd_{50}Bi_1$ structure. Electrochemical evaluation demonstrated that IL/$Pd_{50}Bi_1$ exhibited superior electrocatalytic performance for EOR in alkaline media compared to control samples (Fig. 5(f)). This improved catalytic performance primarily originated from the atomic dispersion of Bi on Pd, which effectively decreased in the activation energy for the rate-limiting step, thus accelerating the overall EOR kinetics. Duchesne et al. [110] synthesized diversified PtAu bimetallic colloidal nanoparticles through a one-step colloidal chemistry approach. The surface composition of these nanoparticles could be precisely controlled to form either Pt atomic clusters or single atoms Pt sites (Fig. 5(g)). Among the synthesized catalysts, Pt_4Au_{96} exhibited stable single-atom Pt catalytic sites, demonstrating exceptional FAOR performance with significantly enhanced activity that surpasses both $Pt_{78}Au_{22}$ and commercial Pt/C catalysts (Figs. 5(h) and 5(i)). DFT calculations provided conclusive evidence that the CO absorbed species on both few-atom and single-atom Pt sites was significantly alleviated, resulting in the effective remission of CO poisoning effects. This finding expanded the potential application range of highly active Pt-based catalysts in various fuel oxidation reactions.

SAAs have confirmed unique structural advantages and catalytic potential in fuel cell small organic molecules oxidation reactions, offering innovative solutions to address the limitations of conventional precious metal catalysts, including high costs, susceptibility to poisoning, and limited stability. For instance, PtRu SAAs exhibited enhanced current density in MOR while effectively mitigating CO poisoning effects through the strong methanol adsorption and weak CO binding at isolated Pt sites [108]. Similarly, the IL/$Pd_{50}Bi_1$ catalyst, featuring atomically dispersed Bi on Pd nanowires, significantly improved EOR kinetics by reducing the activation energy for C–C bond cleavage [109]. In FAOR, the single-atom Pt sites in PtAu bimetallic systems suppressed CO generation pathways, favoring the direct dehydrogenation mechanism and outperforming traditional Pt/C catalysts [110]. These examples highlight that the atomic-scale precision of SAAs enables tailored regulation of reaction pathways and optimized adsorption-desorption dynamics, achieving efficient and stable catalysis in complex multi-electron transfer processes.

4.2 Green electrosynthesis

4.2.1 HER

Hydrogen, a pivotal clean energy carrier, plays an indispensable role in the worldwide transition to sustainable energy systems and decarbonization efforts. The HER is one of the two half-reactions in electrochemical water splitting, with HER serving as the cathode process, represents a promising and environmentally benign approach for green hydrogen production. The construction of effective, durable, and cost-effective HER catalysts is paramount for realizing large-scale water electrolysis for sustainable H_2 generation. The HER mechanism and kinetics are governed by the formation and desorption processes of hydrogen intermediates (H*), where the adsorption/desorption dynamics of H* at catalytic active sites can be quantitatively evaluated through the Gibbs free energy (ΔG_{H*}) of hydrogen adsorption [111]. According to the Sabatier principle, optimal catalytic performance requires a balanced interaction between the catalyst surface and reaction intermediates. Specifically, excessively weak hydrogen adsorption impedes the initial H* formation, while overly strong adsorption hinders subsequent H* desorption [112]. Theoretical and experimental studies have demonstrated that catalysts exhibiting ΔG_{H*} values approaching thermal neutrality ($\Delta G_{H*} \approx 0$ eV) achieve an optimal balance between hydrogen adsorption and desorption, which can maximize the intrinsic HER activity [113]. Among diverse HER catalysts, Pt-based materials have exhibited outstanding HER performance thanks to the optimal ΔG_{H*}, making them prime candidates for sustainable hydrogen production through water electrolysis. However, the widespread implementation of Pt-based catalysts is constrained by the prohibitive cost and limited natural abundance of Pt. Although cost-effective Ni-based electrocatalysts exhibit excellent HER performance with low overpotentials at low current densities, they face significant challenges under high current density conditions, necessitating rational electrode structure design to mitigate bubble-induced energy dissipation [114]. Additionally, the HER activity of Pt materials in alkaline electrolyte demonstrates a significant performance gap, exhibiting 2–3 orders of magnitude lower efficiency compared to that in acidic environments because of the insufficient water dissociation capability. In this context, the development of SAAs presents a promising strategy to minimize noble metal consumption while introducing an activation factor for water cracking, potentially enabling the design of next-generation catalysts with improved atomic efficiency and superior alkaline water electrolysis performance.

Zhao et al. [115] developed an innovative RuBi SAA/Bi@OG nanostructure constituted by alloyed RuBi SAAs and adjacent Bi-O unit dots on oxygen-containing graphene through a one-step pyrolysis process in Fig. 6(a). HAADF-STEM and EDS exhibited the uniform distribution of RuBi SAAs on the graphene surface (Figs. 6(b) and 6(c)), confirming the successful formation of alloyed Bi single atoms and their adjacent Bi-O units. As shown in Fig. 6(d), the modulated RuBi SAA/Bi@OG nanostructure demonstrated exceptional HER catalytic performance in alkaline media, achieving a remarkably

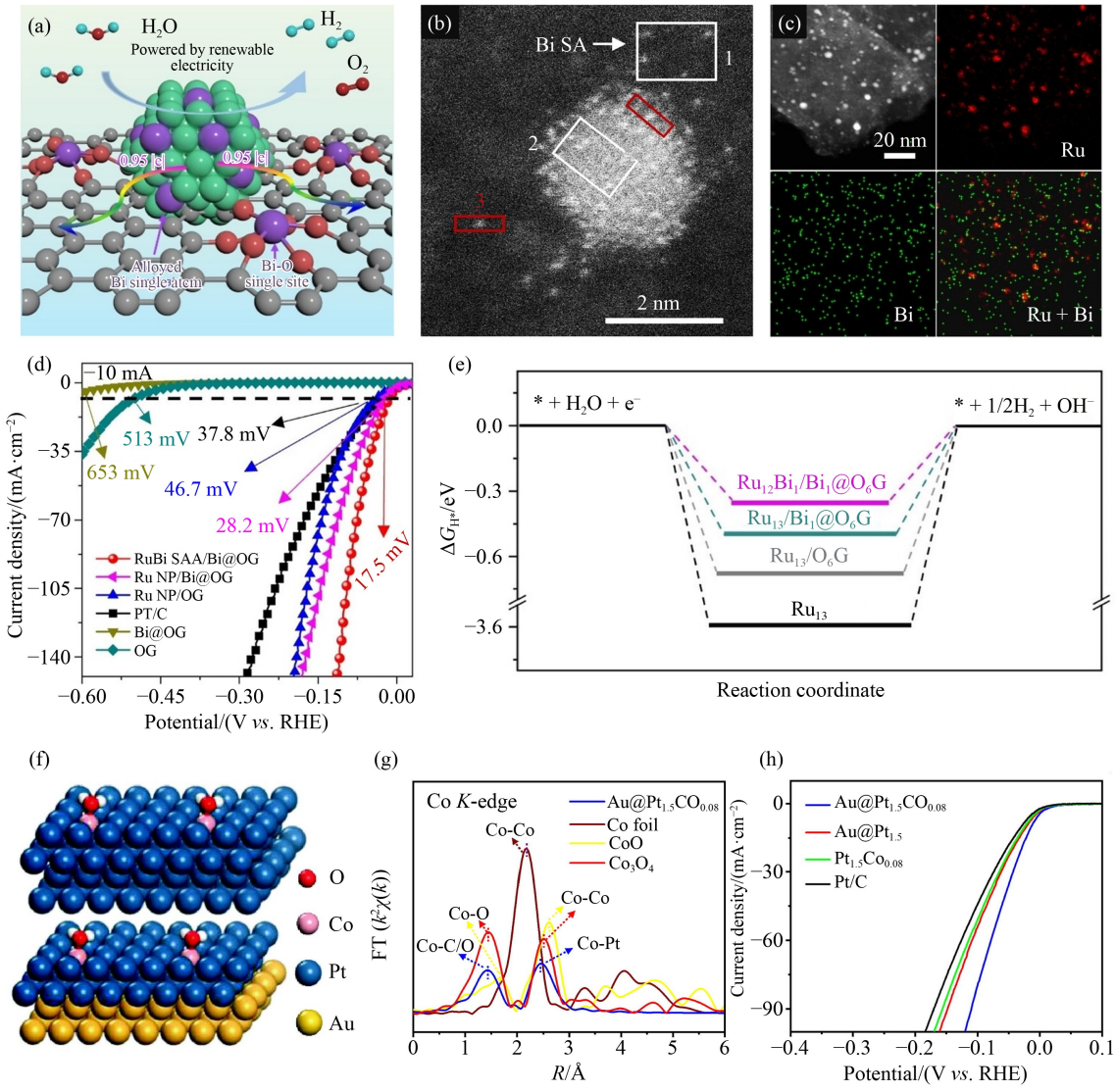

Fig. 6 (a) Schematic illustration of RuBi SAA/Bi@OG. (b) Aberration-corrected HAADF-STEM image of RuBi SAA/Bi@OG. (c) EDS mapping of Ru and Bi in RuBi SAA/Bi@OG. (d) Linear sweep voltammetry (LSV) curves of RuBi SAA/Bi@OG, Ru NP/Bi@OG, Ru NP/OG, Pt/C, Bi@OG, and OG in 1.0 mol·L^{-1} KOH. (e) Calculated ΔG_{H^*} profiles for Ru surface. Reprinted with permission from Ref. [115], copyright 2023, Wiley-VCH. (f) The geometric configurations of the Pt (111) for modeling $Pt_{1.5}Co_{0.08}$ and $Au@Pt_{1.5}Co_{0.08}$. (g) FT of k^2-weighted Co *K*-edge EXAFS of $Au@Pt_{1.5}Co_{0.08}$, Co foil, CoO, and Co_3O_4. (h) LSV curves of various catalysts measured in 1.0 mol·L^{-1} KOH. Reprinted with permission from Ref. [116], copyright 2022, Elsevier.

low overpotential. Notably, the catalyst exhibited an extraordinary mass activity, surpassing most reported HER catalysts. DFT calculations in Fig. 6(e) revealed that the synergistic interplay between the alloyed Bi single atoms and neighboring Bi-O units induces significant surface charge redistribution on Ru sites. This unique electronic configuration enhanced H_2O molecule adsorption on the Ru surface while simultaneously optimizing the free energy of hydrogen adsorption, thus contributing to the superior alkaline HER performance. Wan et al. [116] successfully generated a series of core-shell structured $Au@(PtCo_{0.05})_x$ catalyst (Fig. 6(f)). As shown in Fig. 6(g), EXAFS spectroscopy revealed the absence of Co-Co coordination bonds, providing direct evidence for the atomic dispersion of Co atoms within the Pt substrate. Theoretical and experimental analyses demonstrated that the electronic structure of isolated Co atoms on the Pt shell can be precisely modulated through surface strain effects induced by the Au core, leading to significantly enhanced water dissociation kinetics at the Co active sites. The $Au@Pt_{1.5}Co_{0.08}$ sample exhibited exceptional HER performance in alkaline media, surpassing both commercial Pt/C and $Pt_{1.5}Co_{0.08}$ catalysts (Fig. 6(h)). The superior performance was attributed to the synergistic effects between the strain-modulated electronic configuration and the atomically dispersed Co sites, which collectively regulated the adsorption/desorption properties of reaction intermediates during the HER process.

SAAs successfully address the critical challenges of

conventional Pt-based catalysts in alkaline environments, including high energy barriers for water dissociation and low precious metal utilization, through atomically dispersed active sites design and interfacial electronic modulation. Exemplified by RuBi SAA/Bi@OG and Au@$(PtCo_{0.05})_x$ systems, SAAs achieved precise regulation of ΔG_{H*} via dual-site synergistic mechanisms, delivering exceptional mass activity in alkaline media [115,116]. Theoretical studies reveal that the electronic interactions between isolated metal sites and host matrices in SAAs concurrently optimize hydrogen adsorption energetics and water dissociation kinetics, overcoming the linear scaling limitations inherent to traditional catalysts. With the rapid advancement of green hydrogen technologies, SAAs are poised to emerge as the pivotal materials for overcoming the technical hurdles in alkaline HER, thanks to their atomic efficiency and tunable performance characteristics.

4.2.2 Oxygen evolution reaction (OER)

The OER constitutes a fundamental anodic process in electrochemical energy conversion systems, playing a dual pivotal role as the rate-determining step in water splitting for sustainable hydrogen generation, and an essential component in various electrochemical synthesis applications [117]. This four-electron transfer process not only governs the overall efficiency of proton exchange membrane electrolyzers but also significantly impacts the performance of metal-air batteries and artificial photosynthesis systems [118]. However, OER is characterized by its substantial energy barrier and sluggish kinetics, leading to inherently high overpotentials. The commercial OER catalysis predominantly relies on precious metal-based systems, particularly Ir and Ru compounds, but the exorbitant cost limited natural abundance, and unsatisfactory OER activity hinder the widespread implementation [119]. RuO_2 demonstrates superior cost-effectiveness and enhanced catalytic activity compared to IrO_2, its practical application is constrained by inherent material instability during OER operation. This instability manifests as catalyst dissolution and redeposition processes, ultimately leading to particle agglomeration, specific surface area reduction, and compromised long-term operational stability [120]. These limitations underscore the pressing need for the design of advanced and efficient OER catalysts.

Yang et al. [121] synthesized rutile-phase RuO_2 nanocrystals doped with Bi single atoms (Bi-RuO_2 SAAO (single-atom alloy oxide)) through advanced phase engineering techniques in Fig. 7(a). The incorporation of Bi single atoms into the highly crystalline RuO_2 lattice was systematically verified using HAADF-STEM (Fig. 7(b)). The resulting Bi-RuO_2 SAAO catalyst demonstrated exceptional OER performance, achieving remarkably low overpotentials in 0.5 $mol \cdot L^{-1}$ H_2SO_4 electrolyte and positioning it among the most advanced RuO_2-based electrocatalysts reported to date (Fig. 7(c)). As illustrated in Fig. 7(d), DFT calculations revealed that the incorporation of Bi_1 optimized the electronic structure by modulating electron density distribution, thereby accelerating the potential-limiting step of the OER process. Furthermore, the Bi_1 dopants were found to effectively suppress the demetallization of surface Ru atoms, significantly enhancing the catalyst's structural stability during operation. These results provided innovative comprehension for the development of high-performance OER electrocatalysts. Wang et al. [122] fabricated $Ir_1Ni@MoO_2$ SAAs catalyst, featuring atomically dispersed Ir atoms anchored on the surface of Ni nanoclusters via Ir-Ni covalent interactions, with the Ni clusters supported on MoS_2 substrates Fig. 7(e). The EXAFS analysis revealed Ir-Ni coordination and the absence of Ir–Ir peaks, further indicating the atomic-level dispersion of Ir species on the Ni nanoclusters, which collectively constituted Ir-Ni SAAs structures (Fig. 7(f)). The $Ir_1Ni@MoO_2$ catalyst exhibited exceptional OER performance under alkaline conditions compared to other catalysts in Fig. 7(g). Comprehensive *in situ* characterization combined with DFT calculations revealed that the atomic Ir modification facilitates surface reconstruction of Ni species, leading to enhanced adsorption of hydroxyl intermediate species. Moreover, the presence of Ir single atoms significantly reduced the potential of the rate-determining step in the OER process, thereby improving the overall catalytic efficiency.

SAAs effectively lower the energy barrier for the OER and boost intrinsic activity by precisely regulating the electronic environment and coordination configuration of active sites. For example, Bi single atoms embedded in the RuO_2 lattice accelerated the kinetics of the rate-determining step through charge redistribution [121], while the Ir-Ni single-atom interface reconstructed active surfaces by promoting hydroxyl intermediate adsorption [122]. Most significantly, the SAAs system adeptly balances the conflict between catalytic activity and stability. On one hand, the local electron redistribution induced by single-atom doping optimizes the adsorption energies of oxygen-containing intermediates and lowers the energy barrier for the rate-determining step. On the other hand, the robust interactions between the host and dopant metals prevent the dissolution and aggregation of the active components, markedly prolonging the catalyst's lifespan. The strategic design of SAAs not only overcomes the cost-performance constraints of conventional noble metal catalysts in OER but also opens new avenues for boosting the performance of non-precious metal catalytic systems.

4.2.3 CO_2RR

The electrochemical CO_2RR maintains pivotal signifi-

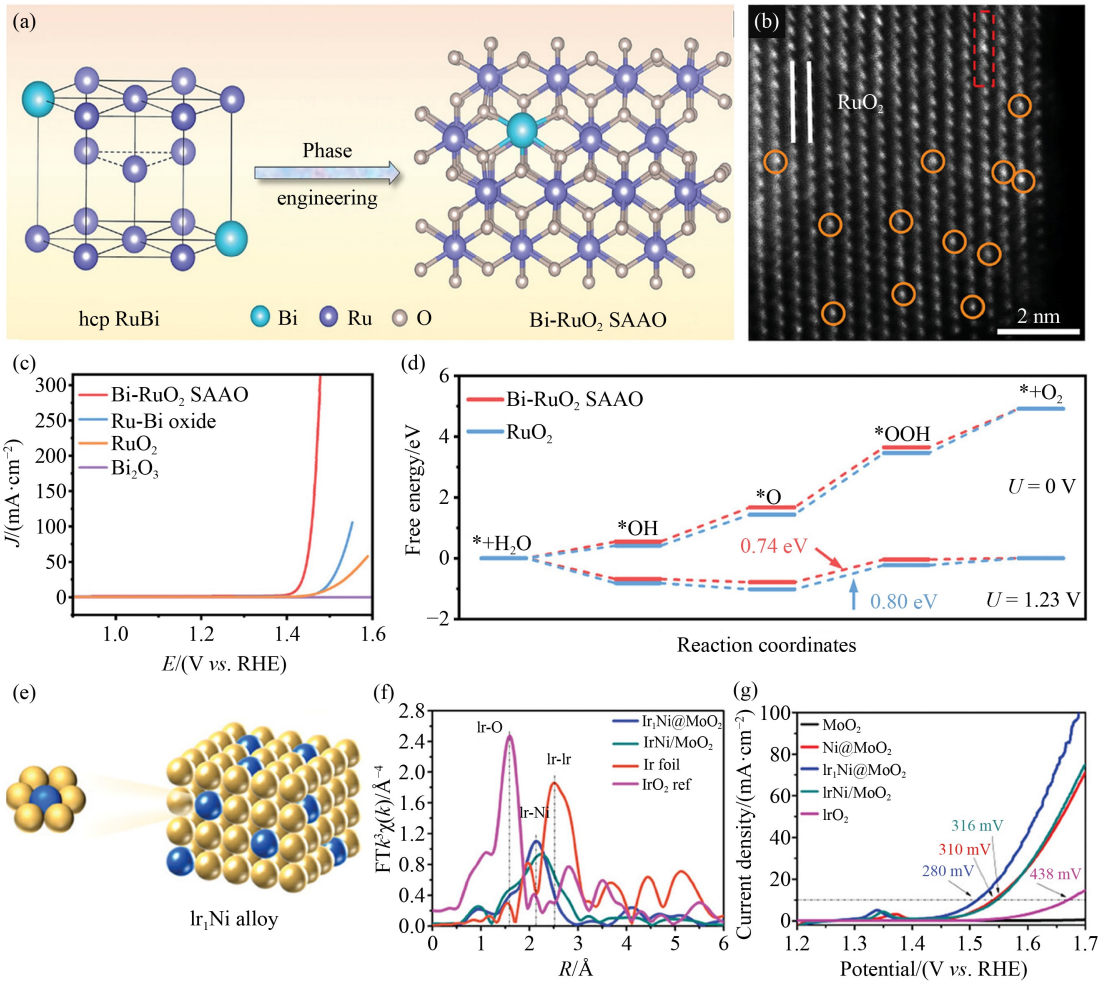

Fig. 7 (a) Schematic depiction of the design and fabrication process for Bi-RuO_2 SAAO. (b) Aberration-corrected HAADF-STEM image of Bi-RuO_2 SAAO. (c) LSV curves of various catalysts measured in O_2-saturated 0.5 mol·L^{-1} H_2SO_4. (d) Calculated free energy profiles for the OER following the adsorbate evolution mechanism pathway on the RuO_2 and Bi-RuO_2 SAAO (110) surface. Reprinted with permission from Ref. [121], copyright 2025, Wiley-VCH. (e) The schematic of the $Ir_1Ni@MoO_2$ SAAs heterostructure. (f) The k^3-weighted EXAFS spectra of $Ir_1Ni@MoO_2$ and $IrNi/MoO_2$, compared with reference spectra of Ir foil and IrO_2. (g) Polarization curves depicting the OER performance of MoO_2, $Ni@MoO_2$, $Ir1Ni@MoO_2$, $IrNi/MoO_2$, and commercial IrO_2. Reprinted with permission from Ref. [122], copyright 2023, Wiley-VCH.

cance in enabling carbon cycle closure and advancing green chemistry by utilizing renewable electricity to transform CO_2 into high-value-added fuels and chemicals. Nevertheless, the CO_2RR represents a highly complex reaction mechanism involving multiple proton-coupled electron transfer steps, with diverse reaction pathways encompassing 2 to 18 electron transfers, leading to a broad distribution of reduction products. These products are capable of being categorized into C_1 species (e.g., CO, HCHO, HCOOH, CH_3OH, and CH_4) and C_{2+} compounds (e.g., C_2H_4, C_2H_5OH, CH_3COOH, and CH_3COCH_3) [123]. Among electrocatalytic materials, Cu has garnered extensive research attention owing to its distinctive capability to reduce CO_2 to hydrocarbons and oxygenates. However, unmodified Cu catalysts face significant challenges, including poor product selectivity, limited stability, and high overpotentials, which collectively hinder the industrial-scale production of C_{2+} products. Therefore, precise regulation of key intermediates at the catalytic active sites and optimization of their binding energies are crucial for controlling the C–C coupling pathway and achieving targeted product selectivity [124].

Wang et al. [125] developed two Cu-based catalyst systems (AgCu NW and Ag_1Cu NW, respectively) by engineering Cu NW with Ag nanoparticles and atomically dispersed Ag atoms, through a galvanic replacement approach, as illustrated in Fig. 8(a). HAADF-STEM imaging indicated the uniform distribution of Ag atoms across the Cu NW surface in Ag_1Cu NW, and Ag existed exclusively in an atomically dispersed state (Fig. 8(b)). Electrochemical performance evaluations revealed that Ag_1Cu NW demonstrated a remarkable Faradaic efficiency (FE) of 56.3% toward ethanol production (Figs. 8(c) and 8(d)). The DFT calculations in Fig. 8(e) elucidated that the enhanced ethanol selectivity in Ag_1Cu

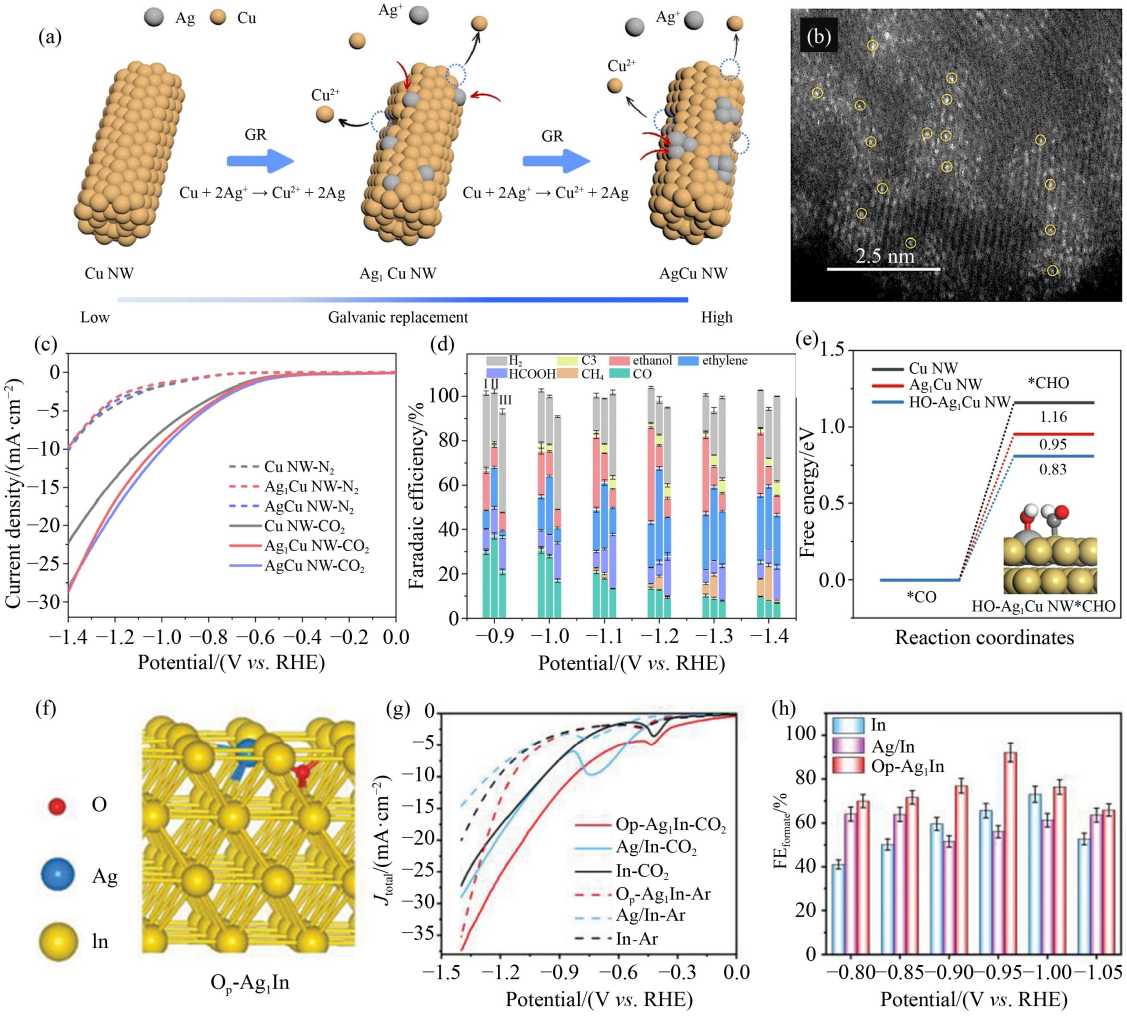

Fig. 8 (a) Schematic diagram illustrating the synthesis process of Ag_1Cu NW and AgCu NW, with Ag represented in gray and Cu in yellow. (b) HAADF-STEM image of Ag_1Cu NW. (c) LSV curves recorded in CO_2- and N_2-saturated 0.1 mol·L^{-1} $KHCO_3$ solution using a rotating disc electrode at a rotation speed of 1600 r·min^{-1}. (d) Potential dependent FE for the CO_2RR on (I) Ag_1Cu NW (left), (II) AgCu NW (middle) and (III) Cu NW (right), measured in an H-type cell. (e) ΔG_{H*} diagrams illustrating the hydrogenation of *CO to *CHO on Cu NW, Ag_1Cu NW and HO-Ag_1Cu NW. Reprinted with permission from Ref. [125], copyright 2024, Springer Nature. (f) The schematic of the Op-Ag1In catalyst. (g) Polarization curves recorded in CO_2- and Ar-saturated 0.5 mol·L^{-1} $NaHCO_3$ electrolyte for Op-Ag1In, Ag/In and In. (h) FE for the CO_2 to formate at different potentials in 0.5 mol·L^{-1} $NaHCO_3$ electrolyte for Op-Ag1In, Ag/In, and In. Reprinted with permission from Ref. [126], copyright 2024, Wiley-VCH.

NW originated from the atomically dispersed Ag sites, which facilitated H_2O dissociation and accelerated the formation of *CO hydrogenation intermediates (*CHO). Furthermore, these Ag single atoms promoted the asymmetric coupling of *CO-*CHO intermediates on adjacent Cu atom pairs. This study provided fundamental insights into the C–C coupling mechanisms underlying C_{2+} product formation and a strategic framework for the systematic design of SAAs catalysts for CO_2RR, containing well-defined active sites to achieve target product selectivity. In another significant study, Fang et al. [126] synthesized an oxygen-pinned stabilization AgIn SAAs (Op-Ag1In) through a mild electrochemical reduction approach in Fig. 8(f). Structural characterization revealed that In elements were uniformly distributed throughout the Op-Ag1In matrix, while Ag and O elements exhibited a discrete distribution pattern. As shown in Figs. 8(g) and 8(h), the Op-Ag1In catalyst demonstrated exceptional electrocatalytic activity toward selective CO_2RR to formic acid, achieving an enhanced FE and optimized partial current densities at –0.95 V (*vs.* RHE). Mechanistic studies revealed that the isolated Ag atoms facilitated the adsorption of key intermediates and substantially enhanced the catalytic performance for CO_2RR to formic acid.

SAAs exhibit distinctive regulatory advantages and promising application potential in the field of electrocatalytic CO_2RR. SAAs enable precise modulation of intermediate adsorption behavior and electron transfer pathways through atomically dispersed active site

engineering, overcoming the limitations of conventional catalysts in product selectivity and reaction kinetics. To illustrate, Ag_1Cu NW significantly enhanced ethanol selectivity by promoting asymmetric coupling of *CO-*CHO intermediates [125], while Op-Ag1In achieved efficient directional formic acid synthesis through optimized adsorption of critical intermediates at isolated Ag sites [126]. These studies elucidated the atomic-level manipulation strategies of SAAs in governing C–C bond formation routes and protonation processes, which maintained the stability of crucial reaction intermediates and concurrently inhibited the aggregation and deactivation of the active components. Such multifunctional characteristics enhance catalytic activity, selectivity, and durability, positioning SAAs as transformative materials for advancing CO_2RR.

4.2.4 Electrochemical synthesis of NH_3

NH_3 plays an indispensable role in modern industry, agriculture, and energy sectors owing to its substantial hydrogen content and high energy density. Currently, the predominant method for NH_3 synthesis is the Haber-Bosch process, which is associated with considerable fossil energy consumption and CO_2 emissions [127]. In alignment with global carbon neutrality objectives, electrochemical NH_3 synthesis has emerged as a prominent research focus in green chemical engineering. This section highlights three primary electrochemical pathways for NH_3 synthesis, including the NRR, nitrite reduction reaction (NO_2RR), and nitrate reduction reaction (NO_3RR).

NRR is considered as an eco-friendly and mild alternative to traditional NH_3 synthesis methods, which facilitates the direct reduction of nitrogen to NH_3 under typical atmospheric conditions. However, NRR faces several challenges, including the inherent inertness of N_2, the substantial energy required for breaking N≡N bond, low N_2 solubility in aqueous electrolytes, and competitive HER. These factors collectively result in low NH_3 yields and FE [128]. NO_2RR offers a dual benefit of mitigating NO_2^- pollution and producing valuable NH_3. Compared to gaseous N_2, NO_2^- exhibits lower N=O bond dissociation energy and higher solubility in water, providing kinetic advantages as a nitrogen source. Nevertheless, NO_2RR involves a complex 6-electron transfer process and is hindered by competing HER, leading to unsatisfactory product yield [129]. NO_3RR holds significant promise for environmental remediation and sustainable NH_3 production. This process involves a cascade reaction where NO_3^- is sequentially reduced to NO_2^- and then to NH_3. However, the formation of NO_2^- as an intermediate byproduct can reduce the overall efficiency of NO_3^--to-NH_3 conversion [130]. Achieving precise control over the reaction pathway to promote NH_3 synthesis while suppressing HER represents a formidable challenge. This necessitates the generation of high-performance catalysts and optimization of reaction conditions to advance NO_3RR toward practical applications.

As illustrated in Fig. 9(a), Li et al. [131] constructed a $PdFe_1$ SAAs catalyst by anchoring Fe single atoms onto a Pd metal support. EXAFS analysis revealed a dominant Fe-Pd coordination peak in $PdFe_1$, with the absence of Fe-Fe and Fe-O bonds, confirming the atomic dispersion of Fe in $PdFe_1$ SAAs (Fig. 9(b)). Electrochemical NRR performance evaluation in acid electrolytes confirmed that $PdFe_1$ has superior FE and NH_3 yields at a potential of –0.2 V (*vs*. RHE) (Fig. 9(c)). Through the integration of XAS, *in situ* Raman spectroscopy, and theoretical calculations, the research team identified and verified that the active centers were constituted by Fe single-atom sites in coordination with Pd. This study underscored the significant potential of SAAs as advanced catalysts for NRR applications. Tan's research group [132] achieved the accurate fabrication of a Cu-Zn (np/ISAA-CuZn, np/ISAA: nanoporous intermetallic SAA) catalyst, featuring the highest concentration of isolated Cu-Zn active sites (Fig. 9(d)). FT-EXAFS analysis revealed a slight shift in the main peak of np/ISAA-CuZn compared to Cu foil, indicating altered atomic spacing (Fig. 9(e)). The analysis of the fitting data revealed that the coordination numbers of Cu-Cu and Zn-Zn bonds in np/ISAA-CuZn dropped to zero, confirming the absence of Cu-Cu and Zn-Zn bonds. This structural configuration ensured the complete isolation of Cu and Zn atoms, forming isolated Cu-Zn active sites. The electrochemical NO_2RR performance of np/ISAA-CuZn was systematically evaluated in Fig. 9(f), which exhibited exceptional selectivity of the np/ISAA-CuZn catalyst for NH_3 synthesis across a wide potential range (–0.2 to –0.8 V *vs*. RHE) under neutral conditions, achieving a remarkable FE and high NH_3 yield. *In situ* XAS studies revealed that np/ISAA-CuZn optimized reactant adsorption and accelerated the protonation process, synergistically enhancing the targeted electrocatalytic transformation of NO_2^- to NH_3. Yu and colleagues [133] developed a novel Au_mCu SAAs aerogel (Au_mCu-SAAs) featuring a three-dimensional interconnected network structure, as shown in Fig. 9(g). EXAFS analysis confirmed the presence of Au–Cu coordination, while the absence of Au–Au bonds at distances greater than 2.7 Å demonstrated the isolated dispersion of Au atoms on the Cu substrate (Fig. 9(h)). The Au_mCu SAAs exhibited exceptional electrocatalytic performance for the NO_3RR across a broad potential range. Remarkably, FE of Au_mCu SAAs remained above 90% in electrolytes containing 0.05–1 mol·L^{-1} NO_3^- and the FEs of Au_mCu SAAs in the electrolyte containing 0.01–0.032 mol·L^{-1} nitrate reached ~80% (Fig. 9(i)).

SAAs demonstrate unique structural merits and exceptional catalytic promise in electrochemical NH_3 synthesis, providing innovative strategies to address the

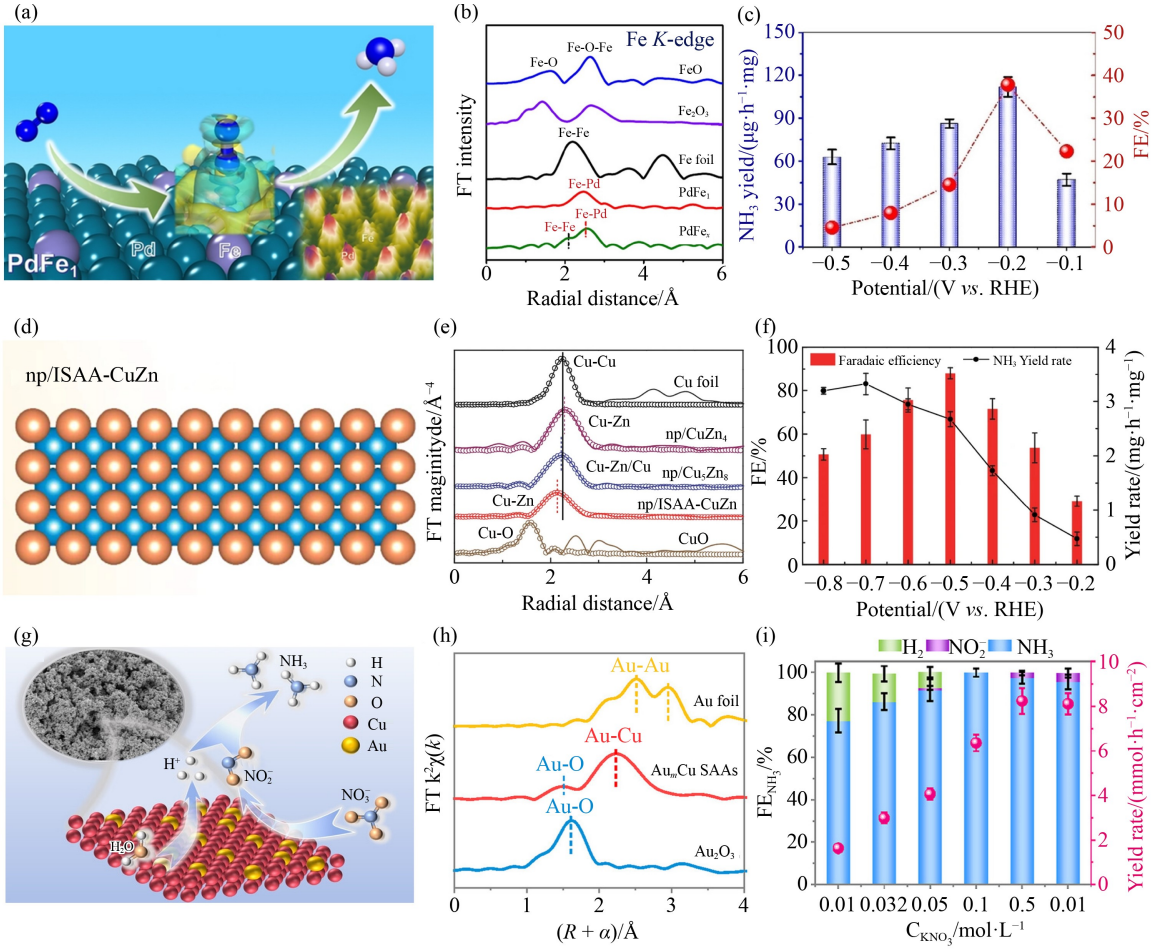

Fig. 9 (a) Schematic illustration of the $PdFe_1$ catalyst. (b) EXAFS spectra of $PdFe_1$, $PdFe_x$, and reference samples of Fe foil, FeO, and Fe_2O_3. (c) The figure shows the calculated NH_3 yield and FEs. Reprinted with permission from Ref. [131], copyright 2022, Wiley-VCH. (d) Schematic diagram illustrating the np/ISAA-CuZn. (e) The corresponding Cu *K*-edge FT-EXAFS spectra of Cu foil, np/$CuZn_4$, np/$CuZn_8$, np/ISAA-CuZn, and CuO. (f) FE and NH_3 yield of np/ISAA-CuZn catalyst at a series of potentials in 0.2 mol·L^{-1} $KHCO_3$ + 1 mmol·L^{-1} KNO_2. Reprinted with permission from Ref. [132], copyright 2024, Springer Nature. (g) The schematic of the Au_mCu SAAs electrocatalyst for the NO_3RR. (h) Au L_3-edge EXAFS spectra in R space for Au_mCu SAAs, Au foil, and Au_2O_3. (i) NO_3RR performances of Au_mCu SAAs at varying NO_3^- concentrations. Reprinted with permission from Ref. [133], copyright 2025, Wiley-VCH.

high energy consumption limitations of conventional production approaches. The atomically dispersed active sites in SAAs allow atomic-level control over nitrogen species adsorption/activation dynamics and proton-electron transfer mechanisms, effectively overcoming fundamental challenges including the high N≡N bond dissociation energy barriers and competitive HER. Research showed that isolated Fe sites in $PdFe_1$ SAAs significantly enhanced NRR activity by optimizing N_2 adsorption configuration [131], while fully isolated Cu-Zn dual sites in np/ISAA-CuZn synergistically promoted directional NO_2^- conversion [132]. The three-dimensional network-structured Au_mCu SAAs achieved efficient NO_3^- reduction through Au-Cu electronic interactions [133]. Therefore, the synthesis of SAAs catalysts with remarkable activity and selectivity provides a forward-looking solution for optimizing electrode materials for nitrogen cycle.

4.2.5 Electrochemical synthesis of high-value-added products

The electrochemical synthesis of high-value-added products achieves synergistic enhancement of atomic economy and energy efficiency through direct integration of renewable electricity with chemical processes. SAAs significantly enhance the selectivity in electrochemical synthesis of high-value-added products by virtue of their unique electronic structures and maximized atomic efficiency. This technological advancement concurrently diminishes fossil fuel dependence and curtails greenhouse emissions inherent to conventional chemical methodologies, thereby directly contributing to energy sustainability. Below are several representative applications of SAAs catalysts in electrochemical synthesis for high-value-added products.

The electrochemical carbon monoxide reduction

reaction (CORR) offers an effective pathway to convert CO from industrial waste gases into high-value C_{2+}. Cu has been extensively studied for its ability to facilitate CO_2/CO conversion to C_{2+}, owing to its unique capability to promote C–C coupling, which is critical for C_{2+} production [134]. Recent advancements have led to the development of Cu-based SAAs (Cu-M, where M=Ag, Pd, Bi), which enhance the surface concentration of *CO intermediates and stabilize the formation of C_{2+} intermediates, thereby improving CORR performance. Sun et al. [135] synthesized Cu-Au SAAs via a one-step reduction method in an aqueous $NaBH_4$ solution using Cu^{2+} and Au^{3+} precursors, resulting in nanoparticles with isolated Au atoms dispersed on a Cu substrate (denoted as $CuAu_{1\%}$). Further modification with N_2SN ligands yielded the $N_2SN/CuAu_{1\%}$ catalyst (Fig. 10(a)). The authors systematically evaluated the CORR performance of the catalysts, revealing that $N_2SN/CuAu_{1\%}$ exhibited significantly higher $FE_{acetate}$ and corresponding $j_{acetate}$ compared to $CuAu_{1\%}$ across all tested current densities in Fig. 10(b). Moreover, $N_2SN/CuAu_{1\%}$ demonstrated superior performance in the yield of C_{2+} compounds in Fig. 10(c). DFT calculations revealed that the N_2SN functional groups simultaneously reduced the energy barrier for C–C bond formation, enhanced CORR activity and selectivity, and suppressed the competing HER.

Urea is a vital chemical product and the most widely used nitrogen fertilizer globally. Developing environmentally friendly and energy-efficient methods for urea production holds substantial importance. Electrochemical methods for urea production have gained attention as a sustainable alternative, supporting the principles of green chemistry and advancing sustainable development objectives. By leveraging the electrochemical co-reduction of CO_2 and NO_3^-, this approach addresses dual challenges of nitrogen-containing wastewater treatment and excessive CO_2 emissions [136]. Dou's team [137] reported an efficient urea electrosynthesis catalyst using CuAu SAAs supported on CeO_2 ($Cu_1Au_8@CeO_2$) with strong

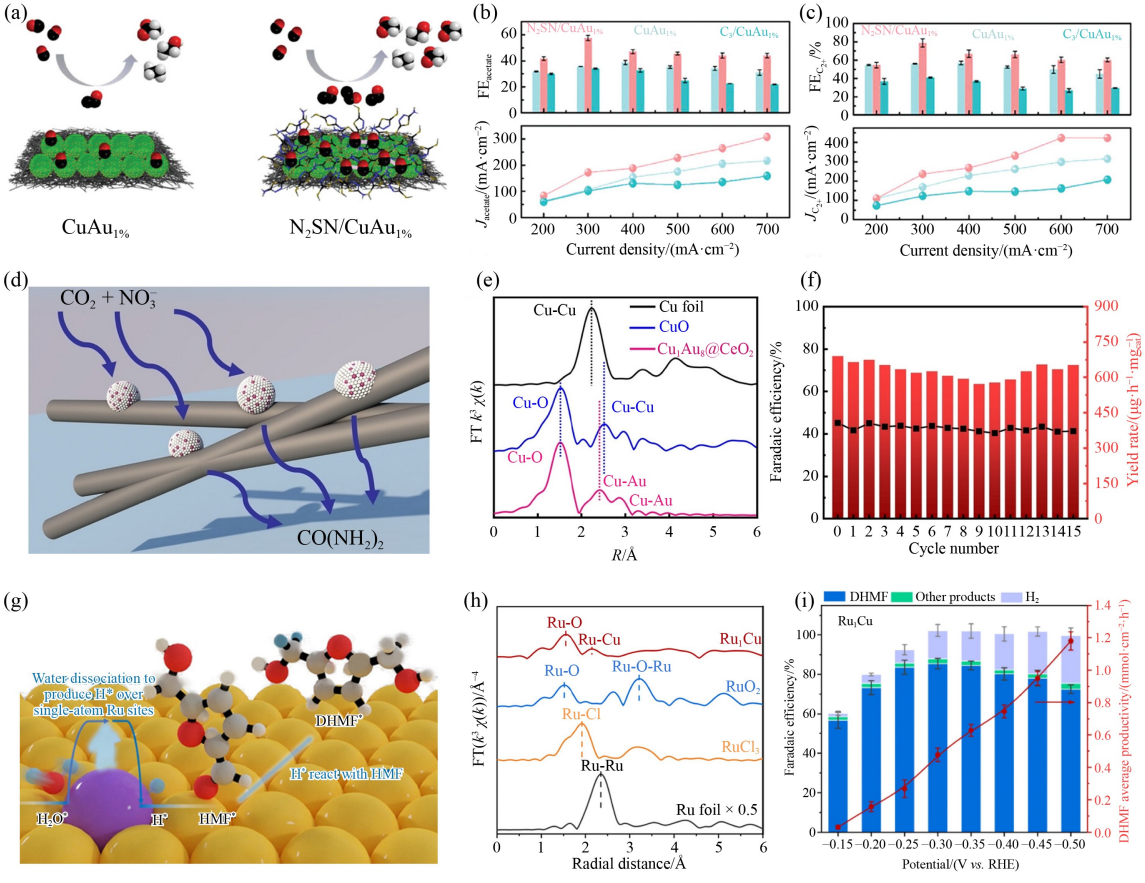

Fig. 10 (a) The illustrations of CORR on $CuAu_{1\%}$ and $N_2SN/CuAu_{1\%}$. (b) CO-to-acetate conversion performance and (c) CO-to-C_{2+} product performance at different current densities for $CuAu_{1\%}$, $N_2SN/CuAu_{1\%}$, and $C_3/CuAu_{1\%}$. Reprinted with permission from Ref. [135], copyright 2024, Wiley-VCH. (d) The schematic illustrates the configuration of CuAu SAA supported on CeO_2 nanorods for the efficient electrosynthesis of urea from NO_3^- and CO_2. (e) FT-EXAFS spectra of Cu foil, CuO, and $Cu_1Au_8@CeO_2$ samples. (f) The stability of $Cu_1Au_8@CeO_2$ for urea synthesis was evaluated at a constant potential of –0.74 V *vs*. RHE. Reprinted with permission from Ref. [137], copyright 2024, Wiley-VCH. (g) The schematic of Ru_1Cu SAA electroreduction toward 5-hydroxymethylfurfural (HMF) (DHMF: 2,5-dihydroxymethylfuran). (h) FT-EXAFS spectra of Ru foil, $RuCl_3$, RuO_2, and Ru_1Cu SAA. (i) The product distributions and average productivity of DHMF over the Ru_1Cu catalyst within a potential range of –0.15 to –0.5 V (*vs*. RHE). Reprinted with permission from Ref. [139], copyright 2022, Wiley-VCH.

electronic metal-support interactions (EMSI) in Fig. 10(d). As illustrated in Fig. 10(e), the absence of Cu-Cu bonds in the EXAFS spectrum confirmed the successful formation of the CuAu SAAs. Electrochemical performance evaluations demonstrated that the $Cu_1Au_8@CeO_2$ catalyst exhibited exceptional efficiency for urea synthesis, with stable urea yield and FE maintained over 15 consecutive cycles in Fig. 10(f). Theoretical and experimental analyses revealed that the atomically dispersed Cu sites in $Cu_1Au_8@CeO_2$ played a critical role in stabilizing key reaction intermediates, facilitating C–N coupling, and enhancing urea selectivity. This work underscored the potential of SAAs catalysts with optimized EMSI for advancing sustainable electrochemical urea synthesis.

Electrochemical reduction of HMF can yield the high value-added chemical DHMF, a high-value chemical precursor for numerous important compounds. However, this process is often hindered by competing HER, leading to reduced FE for DHMF production [138]. Consequently, developing highly effective catalysts for the electrochemical reduction of HMF continues to pose a considerable challenge. As shown in Fig. 10(g), Duan's research group [139] developed a Ru_1Cu SAAs supported on Cu NWAs via a galvanic replacement method, achieving efficient electrocatalytic hydrogenation of HMF to DHMF. The EXAFS spectrum revealed two distinct peaks corresponding to Ru-O and Ru-Cu bonds in Fig. 10(h). The Ru-O bond arose from the unavoidable surface oxidation of Ru in air, while the lack of Ru-Ru bonding interactions confirmed the atomic dispersion of Ru on the Cu NWAs. As demonstrated in Fig. 10(i), the Ru_1Cu catalyst exhibited exceptional FE and selectivity for DHMF production. This advanced efficiency was attributed to the introduction of Ru in atomic-scale, which facilitated H_2O dissociation, generating reactive H* species that efficiently hydrogenated HMF to DHMF through an electrocatalytic hydrogenation mechanism.

Electrochemical synthesis technologies powered by SAA catalysts convert industrial emissions, nitrogen-rich wastewater, and biomass molecules into high-value-added products, facilitating the circular utilization of carbon and nitrogen resources. For instance, Cu-based SAAs efficiently synthesized C_{2+} chemicals in the CORR by enhancing *CO intermediate adsorption and C–C coupling capabilities [135]. Additionally, SAAs catalysts enable the direct electrochemical conversion of industrial waste gases and nitrogen-containing wastewater into urea, overcoming the high-energy-consumption limitations of traditional processes [137]. Moreover, the application of SAAs significantly reduces energy consumption and carbon footprint in biomass conversion, driving the low-carbon transformation of waste biomass into high-value-added chemicals [139]. In conclusion, the widespread adoption of SAAs catalysts in the electrochemical synthesis of high-value products provides an efficient and innovative pathway for green chemistry and sustainable energy transition.

5 Challenges and perspectives

In summary, SAAs catalysts, a novel category of interfacial catalysts, have garnered significant attention in the research on electrochemical energy conversion science in recent years. The distinctive structural features integrate the high electrical conductivity and robustness of conventional alloy catalysts with the high atomic effectiveness and exceptional catalytic selectivity of SACs, endowing SAAs with unique geometric and electronic configurations. As a result, SAAs catalysts exhibit remarkable electrocatalytic performance in various interfacial reactions. Despite substantial progress in laboratory-scale research, the practical application of SAAs still faces numerous challenges that must be overcome to realize their full potential.

5.1 Challenges in scaling up production and industrial utilization

Currently, the synthesis of SAAs is predominantly conducted in laboratory settings using conventional methods such as chemical reduction and galvanic replacement. Although these techniques have proven effective for small-scale SAAs production, the harsh requirements for experimental conditions and high cost greatly restrict large-scale application. Consequently, scaling up SAAs production from laboratory-based synthesis to industrial-level manufacturing presents substantial hurdles. Firstly, industrial reaction environments are inherently more complex, involving multiphase reaction systems, higher reactant concentrations, and extended reaction durations, which impose stricter demands on the stability and catalytic performance of SAAs. Secondly, a critical challenge in scaling up the production of catalysts from laboratory to industrial levels lies in maintaining atomic-level dispersion and structural uniformity throughout the process. Additionally, the mass production process necessitates addressing key engineering aspects, including reactor design, optimization of process parameters, and enhancement of production efficiency. Addressing these challenges will not only enhance the practical utilization of SAAs but also facilitate their wider adoption in industrial catalysis, energy conversion, and environmental applications.

5.2 Indispensable advances *in situ* spectroscopy techniques

Although advanced microscopy and spectroscopy techniques have been extensively employed to

characterize the morphological and electronic architectures of SAAs catalysts. However, significant challenges remain in understanding the dynamic changes in their electronic structure and coordination environment during actual electrochemical reactions. This is primarily attributable to the limitations of existing characterization techniques, as conventional methods are typically performed under static or non-operational conditions, which makes it challenging to accurately capture the dynamic alterations occurring at active sites throughout the reaction process. To address these limitations, *in situ* monitoring approaches are undoubtedly the most effective approaches, which enable the observation of the progressive transformation of reactive sites during electrochemical processes, including the formation and deactivation mechanisms of active centers, the selective regulation of reaction pathways, and coordination environment adjustments. Such detailed insights will significantly advance our understanding of the intrinsic mechanisms governing SAAs' performance in electrochemical reactions.

5.3 Complexities in real-time tracking of isolated active sites

Characterizing adsorbates and their catalytic behavior at isolated single atoms represents a critical scientific challenge in the study of SAAs. The catalytic performance of SAAs is highly dependent on the local coordination environment and electronic structure of these isolated single atoms, making the precise detection of adsorbates and their dynamic evolution essential for elucidating the underlying catalytic mechanisms. However, despite the widespread use of characterization methods such as infrared spectroscopy and Raman spectroscopy to probe surface functional groups and the evolution of reaction intermediates during catalysis, significant challenges remain in characterizing isolated single atoms. A primary issue is that the host metals of SAAs often generate intense spectral signals, which tend to overshadow the local coordination environment around the isolated atoms and the weak signal of the adsorbed species, leading to significant challenges when characterizing isolated single atoms. These limitations in experimental hinder the direct correlation of experimental results with theoretical simulations, and it becomes challenging to confirm the accuracy of these theoretical predictions. Moreover, the inability to definitively assign catalytic roles to specific active sites which limits a comprehensive understanding of the catalytic activity of SAAs.

5.4 Implementing high-throughput screening

It is highly impractical to experimentally synthesize and characterize all potential SAAs candidates due to the expansive design space of SAAs, which encompasses diverse metal combinations, support materials, and varying coordination environments. Therefore, the rapid and efficient identification of SAAs with superior catalytic performance poses a significant challenge. The application of efficient computational methods, such as computational analysis and machine learning has proven to be a crucial strategy for screening and designing high-performance SAAs catalysts. The integration of computational modeling and machine learning not only drastically cuts the expenses and duration associated with experimental trials but also provides profound insights into the structure-performance interplay between the geometric structure, electronic features, and catalytic effectiveness of SAAs.

Competing interests The authors declare that they have no competing interests.

Acknowledgements This work is supported by the National Natural Science Foundation of China (Grant No. 22208322), the Natural Science Foundation of Henan, China (Grant No. 242300421230), and the fund from the State Key Laboratory of Powder Metallurgy, China (Grant No. Sklpm-KF-021).

References

1. Xie B, Wang L, Li H, Huo H, Cui C, Sun B, Ma Y, Wang J, Yin G, Zuo P. An interface-reinforced rhombohedral Prussian blue analogue in semi-solid state electrolyte for sodium-ion battery. Energy Storage Materials, 2021, 36: 99–107
2. Jiao K, Xuan J, Du Q, Bao Z, Xie B, Wang B, Zhao Y, Fan L, Wang H, Hou Z, et al. Designing the next generation of proton-exchange membrane fuel cells. Nature, 2021, 595(7867): 361–369
3. Yan D, Mebrahtu C, Wang S, Palkovits R. Innovative electrochemical strategies for hydrogen production: from electricity input to electricity output. Angewandte Chemie International Edition, 2023, 62(16): e202214333
4. Feng W, Yuan J, Gao F, Weng B, Hu W, Lei Y, Huang X, Yang L, Shen J, Xu D, et al. Piezopotential-driven simulated electrocatalytic nanosystem of ultrasmall MoC quantum dots encapsulated in ultrathin N-doped graphene vesicles for superhigh H_2 production from pure water. Nano Energy, 2020, 75: 104990
5. Chen Z, Yun S, Wu L, Zhang J, Shi X, Wei W, Liu Y, Zheng R, Han N, Ni B. Waste-derived catalysts for water electrolysis: circular economy-driven sustainable green hydrogen energy. Nano-Micro Letters, 2023, 15(1): 4
6. Gao X, Wang P, Sun X, Jaroniec M, Zheng Y, Qiao S. Membrane-free water electrolysis for hydrogen generation with low cost. Angewandte Chemie International Edition, 2025, 64(6): e202417987
7. Fan L, Deng H, Zhang Y, Du Q, Leung D Y C, Wang Y, Jiao K. Towards ultralow platinum loading proton exchange membrane fuel cells. Energy & Environmental Science, 2023, 16(4): 1466–1479

8. Zhuang Z, Li Y, Yu R, Xia L, Yang J, Lang Z, Zhu J, Huang J, Wang J, Wang Y, et al. Reversely trapping atoms from a perovskite surface for high-performance and durable fuel cell cathodes. Nature Catalysis, 2022, 5(4): 300–310
9. Wang N, Jiang W, Yang J, Feng H, Zheng Y, Wang S, Li B, Heng J Z X, Ong W C, Tan H, et al. Contact-electro-catalytic CO_2 reduction from ambient air. Nature Communications, 2024, 15(1): 591
10. Zhao C, Wang Y, Li Z, Chen W, Xu Q, He D, Xi D, Zhang Q, Yuan T, Qu Y, et al. Solid-diffusion synthesis of single-atom catalysts directly from bulk metal for efficient CO_2 reduction. Joule, 2019, 3(2): 584–594
11. Fang H, Liu D, Luo Y, Zhou Y, Liang S, Wang X, Lin B, Jiang L. Challenges and opportunities of Ru-based catalysts toward the synthesis and utilization of ammonia. ACS Catalysis, 2022, 12(7): 3938–3954
12. Xie M, Dai F, Guo H, Du P, Xu X, Liu J, Zhang Z, Lu X. Improving electrocatalytic nitrogen reduction selectivity and yield by suppressing hydrogen evolution reaction via electronic metal-support interaction. Advanced Energy Materials, 2023, 13(21): 2203032
13. Duan W, Li Y, Ou Y, Tuo H, Tian L, Zhu Y, Fu H, Zheng W, Feng C. Insights into electrochemical nitrate reduction to nitrogen on metal catalysts for wastewater treatment. Environmental Science & Technology, 2025, 59(6): 3263–3275
14. Wan Y, Pei M, Tang Y, Liu Y, Yan W, Zhang J, Lv R. Interfacial water regulation for nitrate electroreduction to ammonia at ultralow overpotentials. Advanced Materials, 2025, 37(8): 2417696
15. Govindarajan N, Kastlunger G, Heenen H H, Chan K. Improving the intrinsic activity of electrocatalysts for sustainable energy conversion: where are we and where can we go? Chemical Science, 2021, 13(1): 14–26
16. Yuan J, Wang P, Song N, Wang Y, Ma J, Xiong S, Li X, Feng J, Xi B. Alloying strategy regulating size and electronic structure of $Mo_{0.25}Nb_{0.75}Se_2$ to achieve high-performance lithium-sulfur batteries. Angewandte Chemie International Edition, 2024, 64(9): e202420866
17. Okatenko V, Loiudice A, Newton M A, Stoian D C, Blokhina A, Chen A N, Rossi K, Buonsanti R. Alloying as a strategy to boost the stability of copper nanocatalysts during the electrochemical CO_2 reduction reaction. Journal of the American Chemical Society, 2023, 145(9): 5370–5383
18. Zhang R, Pan L, Guo B, Huang Z, Chen Z, Wang L, Zhang X, Guo Z, Xu W, Loh K P, et al. Tracking the role of defect types in Co_3O_4 structural evolution and active motifs during oxygen evolution reaction. Journal of the American Chemical Society, 2023, 145(4): 2271–2281
19. Ma W, Yao J, Xie F, Wang X, Wan H, Shen X, Zhang L, Jiao M, Zhou Z. Optimizing electronic structure through point defect engineering for enhanced electrocatalytic energy conversion. Green Energy & Environment, 2025, 10(1): 109–131
20. Zhao J, Wang H, Feng L, Zhu J, Liu J, Li W. Crystal-phase engineering in heterogeneous catalysis. Chemical Reviews, 2024, 124(1): 164–209
21. Dong C, Wang X, Zhu Z, Zhan C, Lin X, Bu L, Ye J, Wang Y, Liu W, Huang X. Highly selective synthesis of monoclinic-phased platinum-tellurium nanotrepang for direct formic acid oxidation catalysis. Journal of the American Chemical Society, 2023, 145(28): 15393–15404
22. Du G, Fan Y, Jia L, Wang Y, Hao Y, Zhao W, Su Q, Xu B. Sulfur-deficient $CoNi_2S_4$ nanoparticles-anchored porous carbon nanofibers as bifunctional electrocatalyst for overall water splitting. Frontiers of Chemical Science and Engineering, 2023, 17(11): 1707–1717
23. Zhang A, Liang Y, Zhang H, Geng Z, Zeng J. Doping regulation in transition metal compounds for electrocatalysis. Chemical Society Reviews, 2021, 50(17): 9817–9844
24. Yang X, Li X, Huang Y. Single-atom catalysis: a promising avenue for precisely controlling reaction pathways. Frontiers of Chemical Science and Engineering, 2024, 18(7): 79
25. Xie J, Zhang H, Li S, Wang R, Sun X, Zhou M, Zhou J, Lou X, Xie Y. Defect-rich MoS_2 ultrathin nanosheets with additional active edge sites for enhanced electrocatalytic hydrogen evolution. Advanced Materials, 2013, 25(40): 5807–5813
26. Du C, Li P, Zhuang Z, Fang Z, He S, Feng L, Chen W. Highly porous nanostructures: rational fabrication and promising application in energy electrocatalysis. Coordination Chemistry Reviews, 2022, 466: 214604
27. Su J, Musgrave C B III, Song Y, Huang L, Liu Y, Li G, Xin Y, Xiong P, Li M M J, Wu H, et al. Strain enhances the activity of molecular electrocatalysts via carbon nanotube supports. Nature Catalysis, 2023, 6(9): 818–828
28. Lyu Z, Yu S, Wang M, Tieu P, Zhou J, Shi Q, Du D, Feng Z, Pan X, Lin H, et al. NiFe nanoparticle nest supported on graphene as electrocatalyst for highly efficient oxygen evolution reaction. Small, 2024, 20(15): 2308278
29. Xiao Y, Zhang J, Liu T, Xu M, Dong Y, Wang C. Constructing morphologically stable supported noble metal catalysts in heterogeneous catalysis: mechanisms and strategies. Nano Energy, 2024, 129: 109975
30. Zhang J, Xia Z, Dai L. Carbon-based electrocatalysts for advancedenergy conversion and storage. Science Advances, 2015, 1(7): e1500564
31. Liu L, Lu J, Yang Y, Ruettinger W, Gao X, Wang M, Lou H, Wang Z, Liu Y, Tao X, et al. Dealuminated beta zeolite reverses Ostwald ripening for durable copper nanoparticle catalysts. Science, 2024, 383(6678): 94–101
32. Han J, Bai X, Xu X, Bai X, Husile A, Zhang S, Qi L, Guan J. Advances and challenges in the electrochemical reduction of carbon dioxide. Chemical Science, 2024, 15(21): 7870–7907
33. Yu A, Yang Y. Atomically dispersed metal catalysts for oxygen reduction reaction: two-electron *vs*. four-electron pathways. Angewandte Chemie International Edition, 2025, 64(16): e202424161
34. Zheng S, Zhang F, Jiang Y, Xu T, Li H, Guo H, Zhou Y. Advances in catalysts and reaction systems for electro/photocatalytic ammonia production. Frontiers of Chemical Science and Engineering, 2024, 18(10): 112
35. Wang Y, Wang D, Li Y. Rational design of single-atom site electrocatalysts: from theoretical understandings to practical applications. Advanced Materials, 2021, 33(34): 2008151

36. Sun T, Mitchell S, Li J, Lyu P, Wu X, Pérez-Ramírez J, Lu J. Design of local atomic environments in single-atom electrocatalysts for renewable energy conversions. Advanced Materials, 2021, 33(5): 2003075
37. Wang L, Wang H, Lu J. Local chemical environment effect in single-atom catalysis. Chem Catalysis, 2023, 3(4): 100492
38. Liang X, Fu N, Yao S, Li Z, Li Y. The progress and outlook of metal single-atom-site catalysis. Journal of the American Chemical Society, 2022, 144(40): 18155–18174
39. Zhang T, Walsh A G, Yu J, Zhang P. Single-atom alloy catalysts: structural analysis, electronic properties, and catalytic activities. Chemical Society Reviews, 2021, 50(1): 569–588
40. Sun X, Song Y, Jiang G, Lan X, Xu C. Fundamentals and catalytic applications of single-atom alloys. Science China Materials, 2024, 67(1): 1–17
41. Gao Q, Han X, Liu Y, Zhu H. Electrifying energy and chemical transformations with single-atom alloy nanoparticle catalysts. ACS Catalysis, 2024, 14(8): 6045–6061
42. He C, Gong Y, Li S, Wu J, Lu Z, Li Q, Wang L, Wu S, Zhang J. Single-atom alloys materials for CO_2 and CH_4 catalytic conversion. Advanced Materials, 2024, 36(16): 2311628
43. Jiang B, Zhu J, Xia Z, Lyu J, Li X, Zheng L, Chen C, Chaemchuen S, Bu T, Verpoort F, et al. Correlating single-atomic ruthenium interdistance with long-range interaction boosts hydrogen evolution reaction kinetics. Advanced Materials, 2024, 36(2): 2310699
44. Kyriakou G, Boucher M B, Jewell A D, Lewis E A, Lawton T J, Baber A E, Tierney H L, Flytzani-Stephanopoulos M, Sykes E C H. Isolated metal atom geometries as a strategy for selective heterogeneous hydrogenations. Science, 2012, 335(6073): 1209–1212
45. Hannagan R T, Giannakakis G, Flytzani-Stephanopoulos M, Sykes E C H. Single-atom alloy catalysis. Chemical Reviews, 2020, 120(21): 12044–12088
46. Réocreux R, Stamatakis M. One decade of computational studies on single-atom alloys: is *in silico* design within reach? Accounts of Chemical Research, 2022, 55(1): 87–97
47. Liu J, Wang S, Tian Y, Guo H, Chen X, Lei W, Yu Y, Wang C. Screening of silver-based single-atom alloy catalysts for no electroreduction to NH_3 by DFT calculations and machine learning. Angewandte Chemie International Edition, 2025, 64(2): e202414314
48. Qin F, Chen W. Copper-based single-atom alloys for heterogeneous catalysis. Chemical Communications, 2021, 57(22): 2710–2723
49. Li R, Zhao J, Liu B, Wang D. Atomic distance engineering in metal catalysts to regulate catalytic performance. Advanced Materials, 2024, 36(3): 2308653
50. Darby M T, Sykes E C H, Michaelides A, Stamatakis M. Carbon monoxide poisoning resistance and structural stability of single atom alloys. Topics in Catalysis, 2018, 61(5–6): 428–438
51. Shen T, Wang S, Zhao T, Hu Y, Wang D. Recent advances of single-atom-alloy for energy electrocatalysis. Advanced Energy Materials, 2022, 12(39): 2201823
52. Hannagan R T, Giannakakis G, Réocreux R, Schumann J, Finzel J, Wang Y, Michaelides A, Deshlahra P, Christopher P, Flytzani-Stephanopoulos M, et al. First-principles design of a single-atom-alloy propane dehydrogenation catalyst. Science, 2021, 372(6549): 1444–1447
53. Zhuang J, Wang D. Recent advances of single-atom alloy catalyst: properties, synthetic methods, and electrocatalytic applications. Materials Today Catalysis, 2023, 2: 100009
54. Da Y, Jiang R, Tian Z, Han X, Chen W, Hu W. The applications of single-atom alloys in electrocatalysis: progress and challenges. SmartMat, 2023, 4(1): e1136
55. Liu X, Ao C, Shen X, Wang L, Wang S, Cao L, Zhang W, Dong J, Bao J, Ding T, et al. Dynamic surface reconstruction of single-atom bimetallic alloy under operando electrochemical conditions. Nano Letters, 2020, 20(11): 8319–8325
56. Li J, Zeng H, Dong X, Ding Y, Hu S, Zhang R, Dai Y, Cui P, Xiao Z, Zhao D, et al. Selective CO_2 electrolysis to CO using isolated antimony alloyed copper. Nature Communications, 2023, 14(1): 340
57. Ren W, Tan X, Qu J, Li S, Li J, Liu X, Ringer S P, Cairney J M, Wang K, Smith S C, et al. Isolated copper-tin atomic interfaces tuning electrocatalytic CO_2 conversion. Nature Communications, 2021, 12(1): 1449
58. Giannakakis G, Trimpalis A, Shan J, Qi Z, Cao S, Liu J, Ye J, Biener J, Flytzani-Stephanopoulos M. NiAu single atom alloys for the non-oxidative dehydrogenation of ethanol to acetaldehyde and hydrogen. Topics in Catalysis, 2018, 61(5–6): 475–486
59. Liu J, Shan J, Lucci F R, Cao S, Sykes E C H, Flytzani-Stephanopoulos M. Palladium-gold single atom alloy catalysts for liquid phase selective hydrogenation of 1-hexyne. Catalysis Science & Technology, 2017, 7(19): 4276–4284
60. Ouyang M, Papanikolaou K G, Boubnov A, Hoffman A S, Giannakakis G, Bare S R, Stamatakis M, Flytzani-Stephanopoulos M, Sykes E C H. Directing reaction pathways via *in situ* control of active site geometries in PdAu single-atom alloy catalysts. Nature Communications, 2021, 12(1): 1549
61. Olowoyo J O, Gharahshiran V S, Zeng Y, Zhao Y, Zheng Y. Atomic/molecular layer deposition strategies for enhanced CO_2 capture, utilisation, and storage materials. Chemical Society Reviews, 2024, 53(11): 5428–5488
62. Yang J, Ma D, Li Y, Zhang P, Mi H, Deng L, Sun L, Ren X. Atomic layer deposition of amorphous oxygen-deficient TiO_{2-x} on carbon nanotubes as cathode materials for lithium-air batteries. Journal of Power Sources, 2017, 360: 215–220
63. Jin Z, Xu Y, Chhetri M, Wood J, Torreon B, Che F, Yang M. Recent developments of single atom alloy catalysts for electrocatalytic hydrogenation reactions. Chemical Engineering Journal, 2024, 491: 152072
64. Fonseca J, Lu J. Single-atom catalysts designed and prepared by the atomic layer deposition technique. ACS Catalysis, 2021, 11(12): 7018–7059
65. Wang H, Luo Q, Liu W, Lin Y, Guan Q, Zheng X, Pan H, Zhu J, Sun Z, Wei S, et al. Quasi Pd_1Ni single-atom surface alloy catalyst enables hydrogenation of nitriles to secondary amines. Nature Communications, 2019, 10(1): 4998
66. Zhang L, Liu H, Liu S, Norouzi B M, Song Z, Li J, Yang L, Markiewicz M, Zhao Y, Li R, et al. Pt/Pd single-atom alloys as

highly active electrochemical catalysts and the origin of enhanced activity. ACS Catalysis, 2019, 9(10): 9350–9358

67. Ahmed M, Wang C, Zhao Y, Sathish C I, Lei Z, Qiao L, Sun C, Wang S, Kennedy J V, Vinu A, et al. Bridging together theoretical and experimental perspectives in single-atom alloys for electrochemical ammonia production. Small, 2024, 20(13): 2308084
68. Yan P, Xi S, Peng H, Mitchell D R G, Harvey L, Drewery M, Kennedy E M, Zhu Z, Sankar G, Stockenhuber M. Facile and eco-friendly approach to produce confined metal cluster catalysts. Journal of the American Chemical Society, 2023, 145(17): 9718–9728
69. Lee J, Kwon T, Hyuk K K, Won W, Ro I. Tandem catalysis for plastic depolymerization: *in situ* hydrogen generation via methanol aqueous phase reforming for sustainable polyethylene hydrogenolysis. Angewandte Chemie International Edition, 2025, 64(15): e202420748
70. Wang Y, Zhuang Q, Cao R, Li Y, Gao F, Li Z, He Z, Shi L, Meng Y, Li X, et al. Reduction-controlled atomic migration for single atom alloy library. Nano Letters, 2022, 22(10): 4232–4239
71. Sheng Y, Liu Y, Yin Y, Zou X, Ren J, Wu B, Wang X, Lu X. Rh promotional effects on Pt-Rh alloy catalysts for chemoselective hydrogenation of nitrobenzene to *p*-aminophenol. Chemical Engineering Journal, 2023, 452: 139448
72. Silva A G M, Rodrigues T S, Haigh S J, Camargo P H C. Galvanic replacement reaction: recent developments for engineering metal nanostructures towards catalytic applications. Chemical Communications, 2017, 53: 7135–7148
73. Chung M, Jin K, Zeng J S, Ton T N, Manthiram K. Tuning single-atom dopants on manganese oxide for selective electrocatalytic cyclooctene epoxidation. Journal of the American Chemical Society, 2022, 144(38): 17416–17422
74. Gan T, Shang W, Handschuh W S, Zhang Y, Zhou X. Liquid metal nanoreactor enables living galvanic replacement reaction. Chemistry of Materials, 2024, 36(6): 3042–3053
75. Wang N, Zhao W, Zhang M, Cao P, Sun S, Ma H, Lin M. Bismuth-induced synthesis of Au–*X* (*X* = Pt, Pd) nanoalloys for electrocatalytic reactions. Chemical Communications, 2021, 57(3): 391–394
76. Luo S, Zhang L, Liao Y, Li L, Yang Q, Wu X, Wu X, He D, He C, Chen W, et al. A tensile-strained Pt-Rh single-atom alloy remarkably boosts ethanol oxidation. Advanced Materials, 2021, 33(17): 2008508
77. Zhang X, Cui G, Feng H, Chen L, Wang H, Wang B, Zhang X, Zheng L, Hong S, Wei M. Platinum-copper single atom alloy catalysts with high performance towards glycerol hydrogenolysis. Nature Communications, 2019, 10(1): 5812
78. Liu W, Feng H, Yang Y, Niu Y, Wang L, Yin P, Hong S, Zhang B, Zhang X, Wei M. Highly-efficient RuNi single-atom alloy catalysts toward chemoselective hydrogenation of nitroarenes. Nature Communications, 2022, 13(1): 3188
79. Feng Q, Zhu C, Sheng G, Sun T, Li Y, Zhu Y. Four-dimensional scanning transmission electron microscopy: from material microstructures to physicochemical properties. Acta Physico-Chimica Sinica, 2022, 39(3): 2210017 (in Chinese)
80. Krivanek O L, Chisholm M F, Nicolosi V, Pennycook T J, Corbin G J, Dellby N, Murfitt M F, Own C S, Szilagyi Z S, Oxley M P, et al. Atom-by-atom structural and chemical analysis by annular dark-field electron microscopy. Nature, 2010, 464(7288): 571–574
81. Kwak J H, Hu J, Mei D, Yi C W, Kim D H, Peden C H F, Allard L F, Szanyi J. Coordinatively unsaturated Al^{3+} centers as binding sites for active catalyst phases of platinum on g-Al_2O_3. Science, 2009, 325(5948): 1670–1673
82. Jin C, Lin Y, Wang Y, Shi J, Li R, Liu Y, Yue Z, Leng K, Zhao Y, Wang Y, et al. Engineering atom-scale cascade catalysis via multi-active site collaboration for ampere-level CO_2 electroreduction to C_{2+} products. Advanced Materials, 2025, 37(8): 2412658
83. Mao J, Yin J, Pei J, Wang D, Li Y. Single atom alloy: an emerging atomic site material for catalytic applications. Nano Today, 2020, 34: 100917
84. Varela M, Lupini A R, Benthem K, Borisevich A Y, Chisholm M F, Shibata N, Abe E, Pennycook S J. Materials characterization in the aberration-corrected scanning transmission electron microscope. Annual Review of Materials Research, 2005, 35(1): 539–569
85. Jiang N. Electron beam damage in oxides: a review. Reports on Progress in Physics, 2016, 79(1): 016501
86. Frenkel A I. Applications of extended X-ray absorption fine-structure spectroscopy to studies of bimetallic nanoparticle catalysts. Chemical Society Reviews, 2012, 41(24): 8163–8178
87. Newton M A, Dent A J, Evans J. Bringing time resolution to EXAFS: recent developments and application to chemical systems. Chemical Society Reviews, 2002, 31(2): 83–95
88. Li M, Duanmu K, Wan C, Cheng T, Zhang L, Dai S, Chen W, Zhao Z, Li P, Fei H, et al. Single-atom tailoring of platinum nanocatalysts for high-performance multifunctional electrocatalysis. Nature Catalysis, 2019, 2(6): 495–503
89. Ren H, Yu W, Lv M, Gao J, Hu H, Wang M, Cui X, Liu J, Jiang L. Carbon-encapsulated single-atom platinum nickel alloy for efficient and durable alkaline hydrogen oxidation through enhanced charge polarization. Advanced Functional Materials, 2025, 35(3): 2413754
90. Xing F, Jeon J, Toyao T, Shimizu K, Furukawa S. A Cu-Pd single-atom alloy catalyst for highly efficient NO reduction. Chemical Science, 2019, 10(36): 8292–8298
91. Cao Y, Chen S, Bo S, Fan W, Li J, Jia C, Zhou Z, Liu Q, Zheng L, Zhang F. Single atom Bi decorated copper alloy enables C–C coupling for electrocatalytic reduction of CO_2 into C_{2+} products. Angewandte Chemie International Edition, 2023, 62(30): e202303048
92. Xu Y, Li J, Wu J, Li W, Yang Y, Wu H, Fu H, Zhu M, Wang X, Dai S, et al. Orbital matching mechanism-guided synthesis of Cu-based single atom alloys for acidic CO_2 electroreduction. Advanced Materials, 2025, 37(18): 2500343
93. Wang Y, Han C, Ma L, Duan T, Du Y, Wu J, Zou J, Gao J, Zhu X, Zhang Y. Recent progress of transition metal selenides for electrochemical oxygen reduction to hydrogen peroxide: from catalyst design to electrolyzers application. Small, 2024, 20(22): 2309448

94. Zhang L, Jiang S, Ma W, Zhou Z. Oxygen reduction reaction on Pt-based electrocatalysts: four-electron *vs*. two-electron pathway. Chinese Journal of Catalysis, 2022, 43(6): 1433–1443
95. Sang W, Liu K, Wang T, Lyu J, Nie Z, Zhang L, Xiong M, Li X, Zheng L, Chen C, et al. Nature-inspired diatomic Zn-Cu pairs trigger active two OH* -involved oxygen reduction reaction. Nano Energy, 2025, 138: 110861
96. Peng B, Liu Z, Sementa L, Jia Q, Sun Q, Segre C U, Liu E, Xu M, Tsai Y H, Yan X, et al. Embedded oxide clusters stabilize sub-2 nm Pt nanoparticles for highly durable fuel cells. Nature Catalysis, 2024, 7(7): 818–828
97. Ali A, Laaksonen A, Huang G, Hussain S, Luo S, Chen W, Shen P K, Zhu J, Ji X. Emerging strategies and developments in oxygen reduction reaction using high-performance platinum-based electrocatalysts. Nano Research, 2024, 17(5): 3516–3532
98. Cheng X, Wang Y, Lu Y, Zheng L, Sun S, Li H, Chen G, Zhang J. Single-atom alloy with Pt-Co dual sites as an efficient electrocatalyst for oxygen reduction reaction. Applied Catalysis B: Environmental, 2022, 306: 121112
99. Niu X, Wei J, Xu D, Pei J, Sui R. Charge-asymmetry Fe_1Cu single-atom alloy catalyst for efficient oxygen reduction reaction. Nano Research, 2024, 17(6): 4702–4710
100. Zhang L, Lu P, Yin M, Li R, Wang B, Ma X, Jiao M, Ma W, Zhou Z. Black phosphorus nanodots-modified Pt/C electrocatalyst for methanol-tolerant oxygen reduction in direct methanol fuel cells. Rare Metals, 2025, 44(3): 1767–1776
101. Li Q, Sun C, Sun X, Yin Z, Du Y, Liu J, Luo F. Synthesis of palladium-rare earth alloy as a high-performance bifunctional catalyst for direct ethanol fuel cells. Nano Research, 2024, 17(11): 9525–9531
102. Hu X, An Z, Wang W, Lin X, Chan T, Zhan C, Hu Z, Yang Z, Huang X, Bu L. Sub-monolayer SbO_x on PtPb/Pt nanoplate boosts direct formic acid oxidation catalysis. Journal of the American Chemical Society, 2023, 145(35): 19274–19282
103. Chen W, Cao J, Fu W, Zhang J, Qian G, Yang J, Chen D, Zhou X, Yuan W, Duan X. Molecular-level insights into the notorious CO poisoning of platinum catalyst. Angewandte Chemie, 2022, 134(16): e202200190
104. Wang J, Zhang B, Guo W, Wang L, Chen J, Pan H, Sun W. Toward electrocatalytic methanol oxidation reaction: longstanding debates and emerging catalysts. Advanced Materials, 2023, 35(26): 2211099
105. Yan W, Li G, Cui S, Park G S, Oh R, Chen W, Cheng X, Zhang J, Li W, Ji L, et al. Ga-modification near-surface composition of Pt-Ga/C catalyst facilitates high-efficiency electrochemical ethanol oxidation through a C_2 intermediate. Journal of the American Chemical Society, 2023, 145(31): 17220–17231
106. Chen T, Xu S, Zhao T, Zhou X, Hu J, Xu X, Liang C, Liu M, Ding W. Accelerating ethanol complete electrooxidation via introducing ethylene as the precursor for the C–C bond splitting. Angewandte Chemie International Edition, 2023, 62(38): e202308057
107. Tan X, Wang J, Xiao Y, Guo Y, He W, Du B, Cui H, Wang C. Engineering topological and chemical disorder in Pd sites for record-breaking formic acid electrocatalytic oxidation. Advanced Materials, 2025, 37(4): 2414283
108. Poerwoprajitno A R, Gloag L, Watt J, Cheong S, Tan X, Lei H, Tahini H A, Henson A, Subhash B, Bedford N M, et al. A single-Pt-atom-on-Ru-nanoparticle electrocatalyst for CO-resilient methanol oxidation. Nature Catalysis, 2022, 5(3): 231–237
109. Wang H, Jiao L, Zheng L, Fang Q, Qin Y, Luo X, Wei X, Hu L, Gu W, Wen J, et al. PdBi single-atom alloy aerogels for efficient ethanol oxidation. Advanced Functional Materials, 2021, 31(38): 2103465
110. Duchesne P N, Li Z Y, Deming C P, Fung V, Zhao X, Yuan J, Regier T, Aldalbahi A, Almarhoon Z, Chen S, et al. Golden single-atomic-site platinum electrocatalysts. Nature Materials, 2018, 17(11): 1033–1039
111. Lang C, Xu Y, Yao X. Perfecting HER catalysts via defects: recent advances and perspectives. Chinese Journal of Catalysis, 2024, 64: 4–31
112. Jia Y, Zhang Y, Xu H, Li J, Gao M, Yang X. Recent advances in doping strategies to improve electrocatalytic hydrogen evolution performance of molybdenum disulfide. ACS Catalysis, 2024, 14(7): 4601–4637
113. Xu Q, Zhang J, Zhang H, Zhang L, Chen L, Hu Y, Jiang H, Li C. Atomic heterointerface engineering overcomes the activity limitation of electrocatalysts and promises highly-efficient alkaline water splitting. Energy & Environmental Science, 2021, 14(10): 5228–5259
114. Chen J, Fu G, Tian Y, Li X, Luo M, Wei X, Zhang T, Gao T, Chen C, Chaemchuen S, et al. Three-dimensional-printed Ni-based scaffold design accelerates bubble escape for ampere-level alkaline hydrogen evolution reaction. Interdisciplinary Materials, 2024, 3(4): 595–606
115. Zhao X, Wu G, Zheng X, Jiang P, Yi J, Zhou H, Gao X, Yu Z, Wu Y. A double atomic-tuned RuBi SAA/Bi@OG nanostructure with optimum charge redistribution for efficient hydrogen evolution. Angewandte Chemie, 2023, 135(12): e202300879
116. Wan R, Luo M, Wen J, Liu S, Kang X, Tian Y. Pt-Co single atom alloy catalysts: accelerated water dissociation and hydrogen evolution by strain regulation. Journal of Energy Chemistry, 2022, 69: 44–53
117. Ma Q, Mu S. Acidic oxygen evolution reaction: mechanism, catalyst classification, and enhancement strategies. Interdisciplinary Materials, 2023, 2(1): 53–90
118. Wan R, Yuan T, Wang L, Li B, Liu M, Zhao B. Earth-abundant electrocatalysts for acidic oxygen evolution. Nature Catalysis, 2024, 7(12): 1288–1304
119. Thao N T T, Jang J U, Nayak A K, Han H. Current trends of iridium-based catalysts for oxygen evolution reaction in acidic water electrolysis. Small Science, 2024, 4(1): 2300109
120. Yao Y, Lyu J, Li X, Chen C, Verpoort F, Wang J, Pan Z, Kou Z. A review of efficient electrocatalysts for the oxygen evolution reaction at large current density. DeCarbon, 2024, 5: 100062
121. Yang Z, Ding Y, Chen W, Luo S, Cao D, Long X, Xie L, Zhou X, Cai X, Liu K, et al. Phase-engineered Bi-RuO_2 single-atom alloy oxide boosting oxygen evolution electrocatalysis in proton exchange membrane water electrolyzer. Advanced Materials, 2025, 37(9): 2417777
122. Wang B, Li J, Li D, Xu J, Liu S, Jiang Q, Zhang Y, Duan Z,

Zhang F. Single atom iridium decorated nickel alloys supported on segregated MoO for alkaline water electrolysis. Advanced Materials, 2024, 36(11): 2305437

123. Xu L, Trogadas P, Coppens M O. Nature-inspired electrocatalysts for CO_2 reduction to C_{2+} products. Advanced Energy Materials, 2023, 13(48): 2302974
124. Gomes R J, Kumar R, Fejzić H, Sarkar B, Roy I, Amanchukwu C V. Modulating water hydrogen bonding within a non-aqueous environment controls its reactivity in electrochemical transformations. Nature Catalysis, 2024, 7(6): 689–701
125. Wang S, Li F, Zhao J, Zeng Y, Li Y, Lin Z, Lee T, Liu S, Ren X, Wang W, et al. Manipulating C–C coupling pathway in electrochemical CO_2 reduction for selective ethylene and ethanol production over single-atom alloy catalyst. Nature Communications, 2024, 15(1): 10247
126. Fang C, Huang L, Gao W, Jiang X, Liu H, Hu R, Li X, Yu J, Zhou W. Oxygen-pinned Ag_1In single-atom alloy for efficient electroreduction CO_2 to formate. Advanced Energy Materials, 2024, 14(27): 2400813
127. Chu K, Weng B, Lu Z, Ding Y, Zhang W, Tan R, Zheng Y, Han N. Exploration of multidimensional structural optimization and regulation mechanisms: catalysts and reaction environments in electrochemical ammonia synthesis. Advanced Science, 2025, 12(11): 2416053
128. Li S, Wang Y, Du Y, Zhu X, Gao J, Zhang Y, Wu G. P-block metal-based electrocatalysts for nitrogen reduction to ammonia: a minireview. Small, 2023, 19(16): 2206776
129. Yue L, Song W, Zhang L, Luo Y, Wang Y, Li T, Ying B, Sun S, Zheng D, Liu Q, et al. Recent advance in heterogenous electrocatalysts for highly selective nitrite reduction to ammonia under ambient condition. Small Structures, 2023, 4(11): 2300168
130. Meng X, Tan X, Ma Y, Obisanya A A, Wang J, Xiao Z, Wang D. Recent progress in cobalt-based electrocatalysts for efficient electrochemical nitrate reduction reaction. Advanced Functional Materials, 2025, 35(14): 2418492
131. Li X, Shen P, Luo Y, Li Y, Guo Y, Zhang H, Chu K. PdFe single-atom alloy metallene for N_2 electroreduction. Angewandte Chemie International Edition, 2022, 61(28): e202205923
132. Lan J, Wang Z, Kao C, Lu Y, Xie F, Tan Y. Isolating Cu-Zn active-sites in ordered intermetallics to enhance nitrite-to-ammonia electroreduction. Nature Communications, 2024, 15(1): 10173
133. Yu J, Gao R, Guo X, Truong Nguyen N, Wu L, Wang L. Electrochemical nitrate reduction to ammonia on AuCu single-atom alloy aerogels under wide potential window. Angewandte Chemie International Edition, 2025, 64(4): e202415975
134. Ji Y, Guan A, Zheng G. Copper-based catalysts for electrochemical carbon monoxide reduction. Cell Reports. Physical Science, 2022, 3(10): 101072
135. Sun Q, Tan X, Jia C, Rong C, Wang S, Han C, Xiao Y, Qi H, Smith S C, Zhao C. Molecule doping of atomically dispersed Cu-Au alloy for enhancing electroreduction of CO to C_{2+} products. Advanced Functional Materials, 2024, 34(48): 2406281
136. Ge R, Huo J, Lu P, Dou Y, Bai Z, Li W, Liu H, Fei B, Dou S. Multifunctional strategies of advanced electrocatalysts for efficient urea synthesis. Advanced Materials, 2024, 36(49): 2412031
137. Zhan P, Zhuang J, Yang S, Li X, Chen X, Wen T, Lu L, Qin P, Han B. Efficient electrosynthesis of urea over single-atom alloy with electronic metal support interaction. Angewandte Chemie International Edition, 2024, 63(33): e202409019
138. Jiang Z, Zeng Y, Hu D, Guo R, Yan K, Luque R. Chemical transformations of 5-hydroxymethylfurfural into highly added value products: present and future. Green Chemistry, 2023, 25(3): 871–892
139. Ji K, Xu M, Xu S, Wang Y, Ge R, Hu X, Sun X, Duan H. Electrocatalytic hydrogenation of 5-hydroxymethylfurfural promoted by a Ru_1Cu single-atom alloy catalyst. Angewandte Chemie International Edition, 2022, 61(37): e202209849